

The reaction mechanism of type I phosphomannose isomerases: New information from inhibition and polarizable molecular mechanics studies

Céline Roux,^{1,2} Forum Bhatt,³ Johanna Foret,^{1,2} Benoit de Courcy,^{4,5,6} Nohad Gresh,⁶ Jean-Philip Piquemal,^{4,5} Constance J. Jeffery,³ and Laurent Salmon^{1,2*}

¹Laboratoire de Chimie Bioorganique et Bioinorganique, ICMO, Univ Paris-Sud, UMR 8182, Orsay F-91405, France

²CNRS, UMR 8182, Laboratoire de Chimie Bioorganique et Bioinorganique, ICMO, Orsay, F-91405, France

³Laboratory for Molecular Biology, MC567, Department of Biological Sciences, University of Illinois at Chicago, Chicago, Illinois 60607

⁴UMR 7616, Laboratoire de Chimie Théorique, UPMC Univ Paris 06, F-75252, Paris Cedex 05, France

⁵CNRS, UMR 7616, Laboratoire de Chimie Théorique, F-75252, Paris Cedex 05, France

⁶Laboratoire de Chimie et Biochimie Pharmacologique et Toxicologique, CNRS UMR 8601, Univ Paris Descartes, F-75006, Paris, France

ABSTRACT

Type I phosphomannose isomerases (PMIs) are zinc-dependent metalloenzymes involved in the reversible isomerization of D-mannose 6-phosphate (M6P) and D-fructose 6-phosphate (F6P). 5-Phospho-D-arabinonohydroxamic acid (5PAH), an inhibitor endowed with nanomolar affinity for yeast (Type I) and *Pseudomonas aeruginosa* (Type II) PMIs (Roux et al., *Biochemistry* 2004; 43:2926–2934), strongly inhibits human (Type I) PMI (for which we report an improved expression and purification procedure), as well as *Escherichia coli* (Type I) PMI. Its K_i value of 41 nM for human PMI is the lowest value ever reported for an inhibitor of PMI. 5-Phospho-D-arabinonohydrazide, a neutral analogue of the reaction intermediate 1,2-*cis*-enediol, is about 15 times less efficient at inhibiting both enzymes, in accord with the anionic nature of the postulated high-energy reaction intermediate. Using the polarizable molecular mechanics, sum of interactions between fragments ab initio computed (SIBFA) procedure, computed structures of the complexes between *Candida albicans* (Type I) PMI and the cyclic substrate β -D-mannopyranose 6-phosphate (β -M6P) and between the enzyme and the high-energy intermediate analogue inhibitor 5PAH are reported. Their analysis allows us to identify clearly the nature of each individual active site amino acid and to formulate a hypothesis for the overall mechanism of the reaction catalyzed by Type I PMIs, that is, the ring-opening and isomerization steps, respectively. Following enzyme-catalyzed ring-opening of β -M6P by zinc-coordinated water and Gln111 ligands, Lys136 is identified as the probable catalytic base involved in proton transfer between the two carbon atoms C1 and C2 of the substrate D-mannose 6-phosphate.

Proteins 2011; 79:203–220.
© 2010 Wiley-Liss, Inc.

Key words: competitive inhibitor; hydroxamic acid; metalloenzyme; aldose-ketose isomerase; computational studies.

INTRODUCTION

Phosphomannose isomerases (PMIs, E.C. 5.3.1.8) are metal-dependent aldose-ketose isomerases involved in the reversible isomerization of D-mannose 6-phosphate (M6P) to D-fructose 6-phosphate (F6P) in prokaryotic and eukaryotic cells.¹ PMIs have a substrate specificity for β anomers, namely, β -D-mannopyranose 6-phosphate (β -M6P) and β -D-fructofuranose 6-phosphate (β -F6P) as depicted in Figure 1.² Indeed, α -M6P is a known weak inhibitor of yeast PMI.³ From sequence alignments and physicochemical and kinetic characterizations, it has been proposed that PMIs comprise three families of proteins:

Additional Supporting Information may be found in the online version of this article.

Abbreviations: 5PAA, 5-phospho-D-arabinonate; 5PAH, 5-phospho-D-arabinonohydroxamic acid; 5PAHz, 5-phospho-D-arabinonohydrazide; Ca, *Candida albicans*; Ec, *Escherichia coli*; F6P, D-fructose 6-phosphate; G6P, D-glucose 6-phosphate; G6PDH, D-glucose-6-phosphate dehydrogenase; GDP, guanosine 5'-diphosphate; GMP, GDP-D-mannose pyrophosphorylase; HEI, high-energy intermediate; HEPES, N-(2-hydroxyethyl)piperazine-N'-(2-ethanesulfonic acid); Hs, *Homo sapiens*; M1P, D-mannose 1-phosphate; M6P, D-mannose 6-phosphate; Pa, *Pseudomonas aeruginosa*; PDB, protein data bank; PGI, phosphoglucose isomerase; PMI, phosphomannose isomerase; QC, quantum chemistry; Sc, *Saccharomyces cerevisiae* (yeast); SIBFA, sum of interactions between fragments ab initio computed; St, *Salmonella typhimurium*.

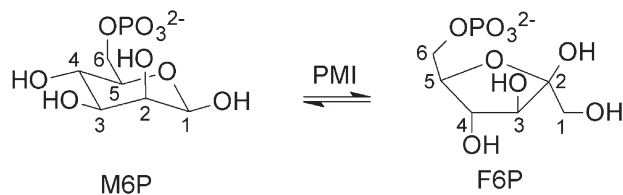
Céline Roux's current address is Département de Botanique et Biologie Végétale, Université de Genève, Sciences III, 30 quai E. Ansermet, CH-1211 Genève 4, Switzerland
Forum Bhatt's current address is Argonne National Laboratories, Biosciences Division, 9700 S. Cass Avenue, Argonne, Illinois 60439.

Grant sponsor: GENCI (CINES/IDRIS) (SIBFA Computations); Grant number: 2009-075009; Grant sponsors: Centre de Ressources Informatiques de Haute Normandie (CRIHAN, Rouen, France) (SIBFA Computations), CNRS (France), Ligue Nationale contre le Cancer (comité Ile-de-France, France), American Heart Association

*Correspondence to: Laurent Salmon, Université Paris-Sud, Laboratoire de Chimie Bioorganique et Bioinorganique, ICMO, UMR 8182, bâtiment 420, 15 rue Georges Clemenceau, Orsay, F-91405, France. E-mail: laurent.salmon@u-psud.fr

Received 2 June 2010; Revised 24 August 2010; Accepted 9 September 2010

Published online 16 September 2010 in Wiley Online Library (wileyonlinelibrary.com). DOI: 10.1002/prot.22873

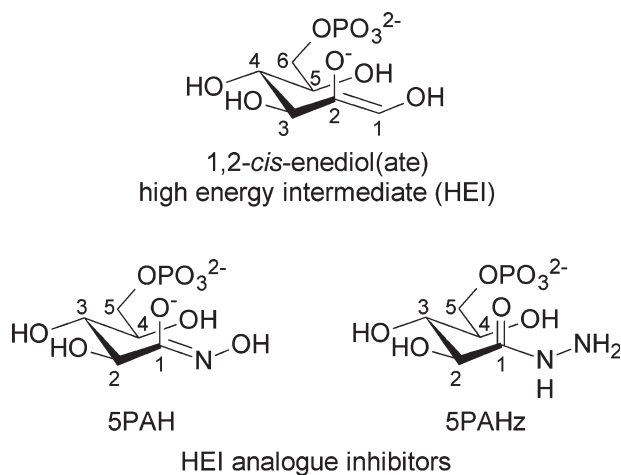
**Figure 1**

Reversible interconversion of M6P and F6P catalyzed by phosphomannose isomerases. Only β -anomers are reported to be substrates of the enzymes.²

Type I, Type II, and Type III families.⁴ Members of each family share little or no sequence identity with members of the other two families, except for a very small conserved amino acid sequence motif, which makes up part of the active site.¹ A fourth type of PMI might be proposed within the phosphoglucose isomerase (PGI, E.C. 5.3.1.9) superfamily, where several aerobic crenarchaeons have been shown to display an atypical dual-specificity PGI/PMI.^{5,6} Type I PMIs are homologous zinc-dependent monofunctional enzymes that catalyze the single reversible isomerization reaction of M6P to F6P and include proteins from *Saccharomyces cerevisiae*,^{4,7–10} *Candida albicans*,^{8,11–14} *Homo sapiens*,⁴ *Escherichia coli*,¹⁵ and *Salmonella typhimurium*,¹⁶ among others. Although F6P is a substrate for glycolysis and gluconeogenesis, production of M6P is the first step of the mannose metabolism pathway which generates guanosine-diphosphate-D-mannose (GDP-D-mannose), the precursor of several mannosylated structures such as fungi cell wall components and bacterial exopolysaccharides.¹⁷ Indeed, PMI activity was reported to be essential for the survival or pathogenesis of bacteria including *Mycobacterium smegmatis*¹⁸ and *Pseudomonas aeruginosa*,¹⁹ the protozoan parasite *Leishmania mexicana*,²⁰ and yeasts including *S. cerevisiae*,²¹ *C. albicans*,²² *Cryptococcus neoformans*,²³ and *Aspergillus nidulans*.²⁴ Although the amino acid sequence of human PMI shares significant identity with those of some pathogenic organisms, we reported the hypothesis that a bitherapeutic approach combining the enzyme inhibitor and D-mannose should alleviate the side-effects of PMI inhibition in humans.²⁵ Consequently, at least in some cases, PMI can be considered as a potential target for the development of antibacterial, antiparasitic, and antifungal agents. The design of such efficient and/or species-specific PMI inhibitors of medical relevance would be much facilitated by more information about the enzyme mechanism of action and the structure of the active site. As detailed below, despite recently reported computational²⁶ and structural¹⁶ studies on PMIs that led to controversial mechanistic conclusions, such information is currently incomplete, and the reaction mechanism still needs to be clarified. On the

basis of new inhibition and theoretical studies as well as on previously reported studies in the literature, our contribution intends to identify all the active site residues and to propose a role for each of them in the reaction mechanism catalyzed by Type I PMIs.

The reversible isomerization reaction between M6P and F6P catalyzed by PMI proceeds through a proton transfer between the two oxygen atoms O1 and O2 and a hydrogen transfer between the two carbon atoms C1 and C2 of the substrate. The latter could proceed either through a “hydride shift mechanism” as reported to occur in the corresponding reactions catalyzed by xylose isomerase^{27–31} and rhamnose isomerase,³² or through a “proton transfer mechanism” via a 1,2-*cis*-enediol(ate) high-energy intermediate (HEI) as observed for triosephosphate isomerase (TIM)³³ and phosphoglucose isomerase (PGI).^{34,35} In the case of yeast Type I PMI, Gracy and Noltmann first argued in favor of a proton transfer mechanism in 1968. From pK_a measurements, a histidine residue was proposed as the catalytic base involved in such a transfer.^{36,37} Thereafter, other studies have confirmed that the Type I PMIs catalyzed isomerization reaction proceeds through a proton transfer mechanism and thus involves a 1,2-*cis*-enediol(ate) HEI as depicted in Figure 2, although the nature of the catalytic base involved in this transfer has not been further discussed. The hydride shift mechanism was rejected on the basis of the temperature dependence of the isotope effect observed for the hydrogen transfer-exchange ratio.³⁸ Tritium exchange data² also supports an enediol mechanism. The pro-S hydrogen on C1 of F6P has been shown to be abstracted during catalysis by PMIs.³⁹ More recently, PMI from *E. coli* in D₂O has been shown to incor-

**Figure 2**

The postulated 1,2-*cis*-enediol(ate) high-energy intermediate (HEI) thought to be involved in the PMI catalyzed reversible isomerization of M6P to F6P is shown with the HEI analogue inhibitors evaluated: 5-phospho-D-arabinonohydroxamic acid (5PAH), here depicted as its hydroximate form, and 5-phospho-D-arabinonohydrazide (5PAHz).

porate deuterium at C1 of the substrate, showing proton exchange to occur between C1H of F6P and the solvent.⁴⁰ Surprisingly, a recent computational study of Type I human PMI argues in favor of a hydride shift mechanism for the hydrogen transfer between the two carbon atoms C1 and C2 of the substrate.²⁶ This mechanistic hypothesis is in disagreement with the generally accepted proposition for PMIs detailed above. Analysis of the figures in the report by Xiao *et al.* suggests that one possibility for the differences in the conclusions might originate from their apparent use of α -D-mannopyranose 6-phosphate, a known yeast PMI inhibitor, instead of the true cyclic substrate β -D-mannopyranose 6-phosphate and L-altrose 6-phosphate instead of D-mannose 6-phosphate.

A high-resolution X-ray crystal structure of the Type I PMI from *C. albicans* (CaPMI, PDB ID code 1PMI), with no substrate or inhibitor bound at the active site, was reported more than 10 years ago.¹² The structure enabled the identification of the location of the active site including the zinc metal cofactor binding site. However, the role of the individual active site amino acids in the isomerization mechanism of M6P to F6P could not be defined. The crystal structures of Type I PMI from *Bacillus subtilis* with a sulfate ion bound (PDB ID code 1QWR),⁴¹ of Type II apo PMI from *Helicobacter pylori* (PDB ID code 2QH5),⁴² and of Type I PMI from *Archaeoglobus fulgidus* (PDB ID code 1ZX5)⁴³ were also deposited, however not described in the literature. In the *B. subtilis* PMI structure, the sulfate ion interacts with residues Lys93, Arg193, and Arg207, which correspond to Gln111, Arg304, and Lys310 in CaPMI, respectively. Recently, structures of the Type I PMI from *S. typhimurium* (StPMI) bound to metal atoms and substrate, together with several bound ethylene glycol molecules, were also reported.¹⁶ With the substrate not directly bound to the zinc atom, the StPMI-Zn-F6P structure (PDB ID code 3H1Y) notably led the authors to identify His99, His131, Lys132, and Asp270 (corresponding to His113, His135, Lys136, and Asp300 in CaPMI, respectively) as the active site residues that could be involved in the ring-opening and isomerization steps of the substrate.¹⁶ Although a detailed mechanism was not given, the authors suggested that the mechanism probably follows the previously proposed *cis*-enediol mechanism that includes proton transfer between C1 and C2 atoms of the substrate. However, the proposed binding site of the substrate F6P is different from that previously proposed by us⁴⁴ and others,¹² and notably does not involve Arg274 (Arg304 in CaPMI), a well-conserved residue among Type I PMIs that was shown to be an active site residue of CaPMI.¹³ No other crystal structure of a PMI enzyme is available, except for those of the crenarchaeons PGI/PMI enzymes, which are likely to be very different from the Types I, II, and III PMIs.^{5,6}

We previously reported strong inhibition of Type I *S. cerevisiae* PMI (ScPMI) by 5-phospho-D-arabinonohy-

droxamic acid (5PAH, Fig. 2), an inhibitor designed as an analogue of the postulated 1,2-*cis*-enediol(ate) high-energy intermediate (HEI, Fig. 2), whereas 5-phospho-D-arabinonate (5PAA) did not inhibit the enzymes.⁴⁵ These studies led us to propose a general mechanism for the isomerization step catalyzed by Type I ScPMI that highlighted a likely catalytic role of the Zn cofactor, rather than only a structural role.⁴⁵ At that time, we proposed that the substrate β -M6P and its corresponding 1,2-*cis*-enediolate HEI were bidentately coordinated to Zn, in accord with the initial mechanistic hypothesis reported by Gracy and Noltmann.³⁶ However, we recently calculated that effective binding of the substrate β -M6P to the catalytic site of CaPMI occurs through binding of the hydroxyl group on C1 of the substrate to the Zn(II)-bound water molecule.²⁵ We also showed that 5PAH binds through its hydroxamate function to the zinc cofactor in a monodentate manner rather than in a bidentate manner.⁴⁴ Although the zinc cofactor can still have a catalytic role, the initial mechanistic hypothesis we proposed is not in accord with these recent theoretical studies. Sagurthi *et al.* also reported that the metal atom plays a role in substrate binding and is important for stabilizing the intermediates formed during catalysis.¹⁶ In the absence of a high-resolution X-ray structure of the enzyme complexed to a HEI analogue inhibitor, a mechanism highlighting the nature and role of the active site residues directly involved at the transition state remains to be proposed.

The polarizable molecular mechanics procedure sum of interactions between fragments *ab initio* computed (SIBFA)⁴⁶ was used to study the PMI-inhibitor interactions.⁴⁴ This procedure was formulated and calibrated on the basis of *ab initio* quantum chemistry (QC). Although QC is a widely used procedure for computation of intermolecular interactions, it cannot be applied routinely to proteins with currently available software. In addition, and to our knowledge, the SIBFA software is the only presently available method to study metalloproteins with an appropriate handling of polarization and charge-transfer contributions involving a metal cation. It was previously applied successfully to various polyligated Zn(II) complexes^{47–54} and provided intermolecular interaction energies with relative errors <3% when compared with QC computations on model complexes.⁵⁵ As mentioned above, we recently reported the SIBFA molecular modeling studies of the enzyme CaPMI complexed with 5PAH or 5PAA,⁴⁴ and with the substrate β -M6P.²⁵ In these preliminary studies, which were not devoted to an investigation of the catalytic mechanism, the three-dimensional structure of the apoenzyme Type I CaPMI (441 residues) was used as a starting point to generate a “SIBFA” 164-residue model of the enzyme based on a 15 Å proximity criteria to Zn(II), and thereafter the different complexes of the model with the inhibitors.

Type I PMIs have been shown to have very similar characteristics with a high level of sequence identity in

the region of the active site,^{4,8} which suggests conclusions that may be drawn from *C. albicans* PMI can most likely be applied to other Type I PMIs, including yeast and *S. typhimurium* PMIs, and human and *E. coli* PMIs studied herein. To clarify the reaction mechanisms of the ring-opening step of the substrate β -M6P and of the subsequent M6P to F6P reversible isomerization catalyzed by Type I PMIs, we report here improved “up-to-date” SIBFA energy-minimized structures of, respectively, the substrate β -anomer of M6P, namely β -D-mannopyranose 6-phosphate (β -M6P), and of the HEI analogue inhibitor 5-phospho-D-arabinonohydroxamate (5PAH, Fig. 2), at the active site of CaPMI. These theoretical structures use the same 164-residue model of CaPMI previously constructed, but include an additional limited array (9 and 11, respectively) of highly polarized discrete water molecules in the binding site. Indeed, the importance of such arrays has been recently demonstrated as they are essential to the modulation of selectivity in a metal binding site⁵⁶ and as their explicit inclusion in the model is mandatory for performing quantitative docking studies⁵⁷ because a sole continuum representation of solvation cannot account for the experimentally observed trends.

We also wish to develop here such mechanistic considerations in relation to a kinetic study of the Type I *E. coli* PMI and the Type I *H. sapiens* PMI (HsPMI), for which we also report an improved method for expression and purification. In addition to the kinetic evaluation of 5PAH on EcPMI and HsPMI, we report the kinetic analysis of 5-phospho-D-arabinonohydrazide (5PAHz, Fig. 2) on both enzymes. 5PAHz is a good inhibitor of PGI, an aldose-ketose isomerase that also uses a proton transfer mechanism but does not contain a metal cofactor at the active site. It had been previously designed in our laboratory to better mimic the neutral 1,2-*cis*-enediol HEI rather than the anionic 1,2-*cis*-enediolate HEI postulated to be involved in the corresponding F6P to G6P isomerization.⁵⁸ Because both PGI and PMI catalytic mechanisms are predicted most likely to involve an analogous HEI, we thought it would be interesting also to evaluate 5PAHz on both Type I PMIs. Altogether, we present here a hypothesis of the overall mechanism for the β -M6P to β -F6P reversible isomerization reaction catalyzed by Type I PMIs based on inhibition studies and polarizable molecular modeling.

MATERIALS AND METHODS

Materials

The disodium salts of 5-phospho-D-arabinonohydroxamic acid (5PAH) and 5-phospho-D-arabinonohydrazide (5PAHz) were synthesized according to reported procedures.^{58–61} M6P was purchased as the barium salt and converted to the sodium salt by ion-exchange chromatography with a Dowex[®]-50X4-400 resin. Purified water

(18.2 M Ω), used for the preparation of the buffer, was obtained by filtration through a Milli-Q device (0.22 μ m) from Millipore. All other commercial chemicals and biochemicals were of reagent grade from Sigma-Aldrich[®] Chemical Company and used without further purification. All solutions and enzyme aliquots were stored at -20°C , except the buffer solution, which was stored at 4°C , and the NADP⁺ solution, which was freshly prepared before use.

Construction of *E. coli* expression vector for human phosphomannose isomerase

A mammalian expression plasmid, pcDNA3.1/GS, containing the gene for human phosphomannose isomerase was purchased from Invitrogen (Carlsbad, CA). For expression in bacteria, the HsPMI gene was transferred to an *E. coli* expression vector. First, the gene was amplified by PCR using primers that replaced seven rare codons to more common codons. The substitutions did not affect the amino acid sequence. The primers used were: Forward primer 5' ATTG **TTCATATGGCGGCGCCGCGCGTGTTC**CCGCTGAGCTGTGCGGTGCAGCAGTATGCCTGGGGGAAGATGGGTTCCA A CAGC 3' (the start site is underlined, and the bases that were changed are highlighted in bold); reverse primer 5' ATTGTTGGATCCTTACAGCAGACAGCAGGCACGGAA TATCAGCAGGTCC 3'. A second PCR step was performed to add the restriction sites *Nde*I and *Bam*HI on the 5' and 3' ends of the gene, respectively, a sequence encoding a hexahistidine tag on the protein's C-terminus, and a stop codon. The hexahistidine tag aids in purification and detection of the expressed protein. The primers used were: Forward primer FHB8 5' TGCTCTTCATATGGCCGCTCCGCGAG TATTCC 3'; reverse primer FHB9 5' CGGGATCCTTA GTGGTGGTGGTGGTGGTGCAGCAGACAGCAGGCACG GAATATCAG 3'. A 1300 bps PCR product was obtained, purified using a PCR product purification kit (Qiagen, Valencia, CA), and digested with *Nde*I and *Bam*HI restriction enzymes (Gibco-Invitrogen, Carlsbad, CA). This digested DNA fragment was ligated into the *Nde*I-*Bam*HI site of vector pLEX (Invitrogen, Carlsbad, CA), and the resulting HsPMI expression plasmid is referred to as pFBPMI. HsPMI protein expression is under the tight regulation of the P_L promoter. The DNA sequence of the insert was checked for mutations.

Expression and purification of human phosphomannose isomerase

pFBPMI was used to transform GI724 competent cells (Invitrogen, Carlsbad, CA). The transformation mixture was plated onto RM-agar plates containing 100 μ g/mL ampicillin and incubated at 30°C (RM-agar plates, 1 L: 20 g Casamino acids, 100 mL $10\times$ M9 salts, 1 mL 1M MgCl₂, 25 mL 20% glucose, 1 mL 100 mg/mL ampicillin, 15 g agar). Starter cultures were grown overnight in RM media, and larger cultures were grown in induction me-

dium (1 L induction medium: 2 g Casamino acids, 100 mL 10× M9 salts, 1 mL 1M MgCl₂, 25 mL 20% glucose, 1 mL 100 mg/mL ampicillin). The culture was grown at 30°C until the OD₆₅₀ reached 0.5. Protein expression was induced by adding L-tryptophan to a final concentration of 100 µg/mL. The culture was grown for a further 4 h at 37°C, and the cells were harvested and frozen at -80°C until further use. A total of 50 g of cells, obtained from 9 L of culture, were thawed on ice and resuspended in 200 mL ice cold binding buffer (0.02M sodium phosphate buffer, pH 8.0, 0.5M NaCl, 5 mM imidazole). CompleteTM EDTA-free protease inhibitor tablets (Roche, Nutley, NJ) were added to the binding buffer before use. The cells were lysed by sonication and centrifuged at 10,000g for 30 min at 4°C to remove cell debris. The cleared supernatant was filtered through a 0.22-µm filter (Millipore) and loaded onto a 5-mL HiTrap metal chelating FPLC column (Amersham Pharmacia, Piscataway, NJ) charged with nickel. The HsPMI eluted at ~0.1M imidazole concentration using a linear gradient of imidazole. The fraction containing HsPMI was dialyzed against 50 mM Tris-HCl, pH 8.0 and then filtered and loaded onto an FPLC Q-sepharose column (Amersham Pharmacia, Piscataway, NJ). The protein eluted at ~0.15M NaCl concentration using a linear gradient of NaCl. The fraction containing active enzyme was dialyzed against 50 mM Tris-HCl, pH 8.0. Approximately 7 mg of pure protein was obtained per 9 L of culture.

Instruments

UV absorbance measurements were made with a Safas 190 DES spectrophotometer equipped with a Julabo thermostat regulation device, using 1 mL Brand polystyrene disposable cuvettes with a 1-cm optical path.

PMI assays using the PGI/G6PDH coupled enzyme method

Human and *E. coli* PMI activities were assayed spectrophotometrically at 340 nm using a coupled enzyme assay with PMI activity coupled to the activities of yeast PGI and yeast D-glucose-6-phosphate dehydrogenase (G6PDH), following a procedure adapted from the literature.^{7,62} Both auxiliary enzymes were added in excess so that the rate-limiting reaction was the PMI-catalyzed isomerization of M6P to F6P. Careful control experiments were conducted to check this assumption by adding further excess of the auxiliary enzymes (5- and 10-fold) in the absence and presence of the inhibitor at its highest concentration. The activity measurements were made using the multicuvettes mode with the temperature held at 25°C. Specific activities were measured using a substrate concentration of at least 5 times the corresponding K_m value. In the case of human PMI, the assay mixture contained, in a volume of 1 mL: 50 mM HEPES buffer, pH 7.1, previously sterilized and fil-

tered (0.22 µm); 20–100 µM M6P sodium salt (100 mM in buffer); 5 mM MgCl₂ (500 mM aqueous solution); 0.4 mM NADP⁺ sodium salt (40 mM in buffer, freshly prepared); 0.6 unit G6PDH (5.2 mg lyophilized protein in 707-µL water; a 5-µL aliquot was diluted to 500 µL with buffer just before use); 0.6 unit PGI (4.4 mg lyophilized protein in 830 µL water, and dilution before use of a 5 µL aliquot to 500 µL with buffer); 0–0.08 µM 5PAH or 0–0.7 µM 5PAHz (100 mM aqueous solutions appropriately diluted 10–10,000 times). Following preincubation in the spectrophotometer compartment until no further increase in absorbance due to substrate occurred (6–7 min), the reaction was initiated by the addition of 0.005 unit of human PMI. In the case of *E. coli* PMI, the enzymatic assay was identical excepted for the following values: 0.2–0.6 mM M6P; 0.6 units G6PDH; 0.6 unit PGI; 0–0.3 µM 5PAH or 0–2 µM 5PAHz; 0.006 unit PMI (10 µL commercial solution diluted 10,000 with buffer). The rate of absorbance change due to NADPH formation ($\epsilon = 6220\text{M}^{-1}\text{cm}^{-1}$) coupled to M6P isomerization was then measured. PGI and G6PDH activities were assayed with F6P and G6P, respectively, using a related protocol, which is described in Refs. 58 and 63. Duplicate kinetic data were analyzed by double reciprocal plots of the initial reaction velocity versus M6P concentration measured at various inhibitor concentrations. Linear least squares fit to the observed data using the Michaelis-Menten equation for competitive inhibition allowed secondary graphical representation of the slope as a function of inhibitor concentration, from which was obtained the value of the inhibition constant (K_i). Units of enzyme activity are defined as micromoles of substrate converted per minute at 25°C under the assay conditions described. All the results reported below were validated by carefully controlled experiments designed to check that the PMI-catalyzed step was indeed the one inhibited by the evaluated inhibitor or, in other words, that the PMI step was rate determining, even at the highest inhibitor concentration used. So, in the conditions we used, neither PGI nor G6PDH is inhibited by the targeted molecule with respect to the inhibition of PMI.

The SIBFA interaction energy formulation

SIBFA is a highly accurate molecular mechanics/molecular dynamics (MM/MD) procedure formulated on the basis of ab initio quantum chemistry (QC), and validated by numerous QC tests on model complexes. Currently, the most widely used approach to model the electrostatic properties uses atom-centred charges that are derived by fitting to the ab initio molecular electrostatic potential. However, a much more accurate representation uses multicentre multipoles derived from ab initio molecular wave functions. The SIBFA molecular mechanics procedure provides a very promising way to calculate refined scoring functions. The SIBFA intermolecular interaction energy E_{int} is formulated as a sum of five contributions

denoting the electrostatic multipolar E_{MTP*} , short-range repulsion E_{rep} , polarization E_{pol} , charge transfer E_{ct} , and dispersion E_{disp} contributions, respectively:

$$E_{int} = E_{MTP*} + E_{rep} + E_{pol} + E_{ct} + E_{disp}$$

The detailed analytical forms of these contributions have been reviewed.⁴⁶ SIBFA enables an accurate calculation of the electrostatic contribution to the intermolecular interaction energy from a multipolar expansion of the electronic distribution (E_{MTP*}) up to quadrupoles. Such multipoles are located on the atoms and on the barycenters of the chemical bonds of the constitutive molecular fragments, and E_{MTP*} is corrected at short-range to take penetration effects into account.⁶⁴ Overall, SIBFA's total energy function is fully separable⁶⁴ as each of the different contribution matches its QC counterpart^{65,66} enabling direct validation tests of SIBFA by parallel QC computations.

On the basis of a 15 Å proximity criterion to Zn(II), we previously created a “SIBFA” 164-residue model protein of the original tri-dimensional crystal structure of CaPMI (PDB ID code 1PMI) reported by Cleasby *et al.*¹² The model protein was assembled with the standard library of its constitutive backbone and side-chain fragments, encompassing the internal coordinates and the distributed multipoles and polarizabilities. The truncated model protein minimized structure, which showed no corresponding differences when compared with the integral protein minimized structure, was used for SIBFA calculations on previous CaPMI-ligand complexes.⁴⁴ The same truncated model of CaPMI is used in the present study, except that additional “discrete” water molecules have been included so that energy calculations and structures obtained are different than we previously reported. Indeed, energy-minimization (EM) is performed, to relax the ligand-protein (L-P) complex in the framework of the SIBFA potential. Automatic location of a “discrete” number of structural water (W) molecules around the accessible polar sites of the L-P complex is done next, using an algorithm due to Claverie *et al.*⁶⁷ and interfaced in the SIBFA software. In a previous study, the number of nine “discrete” water molecules was shown to be sufficient so as to create an adequate network around the malonate-based phosphate surrogate of β -M6P.²⁵ EM is then restarted, first on the water variables, and next upon relaxing the entirety of relevant variables of the L-P-W complex. Details of the EM procedure using SIBFA can be found in the Supporting Information.

RESULTS

Expression and purification of human phosphomannose isomerase

Recombinant expression and purification of HsPMI was reported previously.⁴ We report herein an improved method that yields ~ 7 times more protein than previously

Table I

Inhibition of the M6P to F6P Isomerization Catalyzed by Human and *E. coli* PMIs^a

Inhibitor	Parameter	Human	<i>E. coli</i>
None	K_m (μM)	43 ± 3	330 ± 30
	k_{cat} (s^{-1})	36 ± 1	23 ± 1
	k_{cat}/K_m ($mM^{-1} s^{-1}$)	840 ± 80	70 ± 9
5PAH	K_i (μM)	0.041 ± 0.006	0.08 ± 0.01
	K_m/K_i	1000 ± 200	4100 ± 900
5PAHz	K_i (μM)	0.6 ± 0.1	2.0 ± 0.2
	K_m/K_i	70 ± 20	160 ± 30

^a K_i values were determined using the PGI/G6PDH coupled enzyme assay (see Materials and Methods for details on kinetic assay conditions).

reported, and at $\sim 99\%$ purity (SDS PAGE gel of purified HsPMI can be found in Supporting Information Fig. S1). The previously reported purification method yielded 3.3 mg of HsPMI from 160 g of *E. coli* cells and required an ammonium sulfate precipitation step and seven column chromatography steps. The new purification method described herein makes use of a 6-histidine affinity tag and involves just two chromatography steps: metal affinity chromatography and a Q-sepharose anion exchange column. The new method also results in a much better yield of protein, 7 mg of pure, active human PMI from ~ 50 g of *E. coli* cells.

Kinetic parameters of human and *E. coli* PMI

The values of K_m , k_{cat} , and k_{cat}/K_m for the M6P to F6P isomerization reaction were measured for both recombinantly expressed and purified HsPMI and commercial EcPMI and are reported in Table I. The K_m values of 43 and 330 μM that we determined for HsPMI and EcPMI, respectively, are in the range of the value of 230 μM previously reported for HsPMI in 50 mM Tris-HCl pH 8.⁸ The k_{cat}/K_m ratios of 840 and $70 M^{-1} min^{-1}$ for HsPMI and EcPMI, respectively, determined for the M6P to F6P isomerization reaction, are less than one order of magnitude different from the value reported for ScPMI of $165 M^{-1} min^{-1}$.⁴⁵ Comparison of all these k_{cat}/K_m values for Type I PMIs with the corresponding value determined for Type II PMI from *P. aeruginosa* of $0.030 M^{-1} min^{-1}$ ⁴⁵ supports the hypothesis that Type I PMIs appear to be much more efficient catalysts than Type II PMIs for the reaction in the M6P to F6P direction, with Type I PMIs from eukaryotes being more efficient than the bacterial Type I PMIs. This large efficiency difference between Type I and Type II PMIs is consistent with the fact that, from a metabolic point of view, these two types of enzymes preferentially catalyze the reaction in opposite directions: Type I PMIs consume M6P as a substrate, whereas Type II PaPMI produces it for the alginate biosynthetic pathway.

Inhibition of human and *E. coli* PMI

The 1,2-*cis*-enediol(ate) HEI analogue inhibitors evaluated in this study, namely 5-phospho-D-arabinonohydroxamic acid (5PAH) and 5-phospho-D-arabinonhydrazide

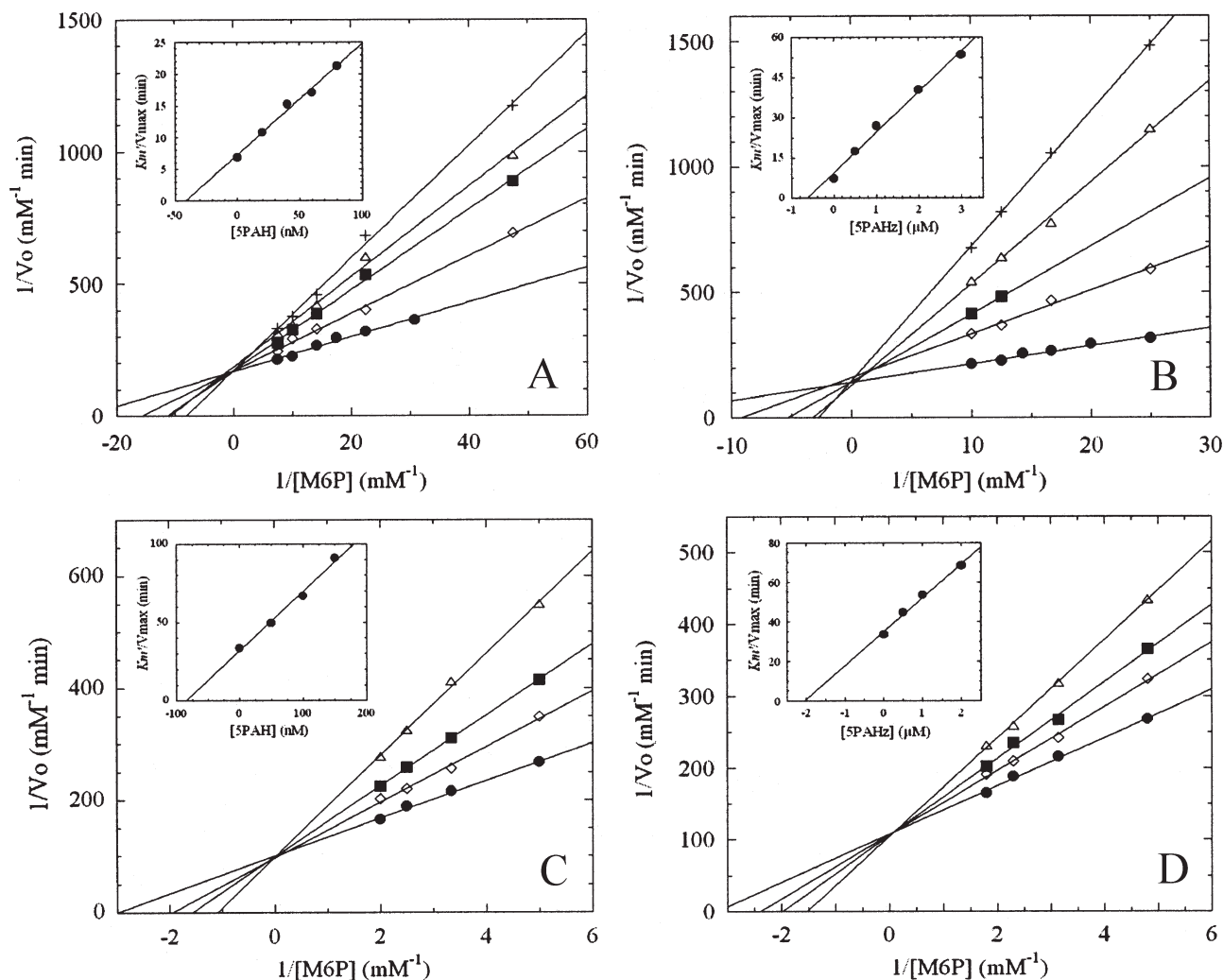


Figure 3

Inhibition of (A) HsPMI by 5-phospho-D-arabinonohydroxamic acid (5PAH), (B) HsPMI by 5-phospho-D-arabinonohydrazide (5PAHz), (C) EcPMI by 5-phospho-D-arabinonohydroxamic acid (5PAH), and (D) EcPMI by 5-phospho-D-arabinonohydrazide (5PAHz) using the PGI/G6PDH coupled enzyme assay method (see Materials and Methods for details on kinetic assay conditions). Double reciprocal plot of the initial reaction velocity versus M6P concentration obtained at various inhibitor concentrations: (A) (●) no inhibitor, (◇) [I] = 20 nM, (■) [I] = 40 nM, (Δ) [I] = 60 nM, and (+) [I] = 80 nM; (B) (●) no inhibitor, (◇) [I] = 0.5 μM, (■) [I] = 1 μM, (Δ) [I] = 2 μM, and (+) [I] = 3 μM; (C) (●) no inhibitor, (◇) [I] = 50 nM, (■) [I] = 100 nM, and (Δ) [I] = 150 nM; (D) (●) no inhibitor, (◇) [I] = 0.5 μM, (■) [I] = 1 μM, and (Δ) [I] = 2 μM. In the inserted secondary plot, the slopes (K_m/K_i) of the straight lines of the primary graphs were plotted against inhibitor concentrations, which gives $-K_i$ for the intercept.

(5PAHz), are depicted in Figure 2. Their inhibitory efficiencies were determined with the three enzymes coupled assay for Type I PMIs and are reported in Table I.

The two new inhibitors of HsPMI, 5PAH and 5PAHz, behave as competitive inhibitors of the enzyme with respect to M6P isomerization [Fig. 3(A,B)] with K_m/K_i ratios of 1000 and 70, respectively. In the case of 5PAH, the K_i value of 0.041 μM is the lowest value ever reported for the human enzyme, as well as for any PMI. As previously observed for ScPMI and PaPMI,⁴⁵ 5PAH appears to be a strong competitive inhibitor of the human enzyme. The large value of the K_m/K_i ratio sug-

gests that the inhibitor structure is more closely comparable to the high-energy intermediate structure than the substrate structure. 5PAH thus behaves as a stable high-energy intermediate analogue inhibitor of the M6P to F6P isomerization reaction. 5PAHz also behaves as a strong competitive inhibitor of HsPMI activity with a K_i value of 0.6 μM. However, the K_m/K_i ratio value of 70 indicates that 5PAHz is about one order of magnitude less efficient than 5PAH.

5PAH and 5PAHz also behave as two new competitive inhibitors of EcPMI [Fig. 3(C,D)], with respective K_i values of 0.08 and 2.0 μM. Although 5PAH is a much stron-

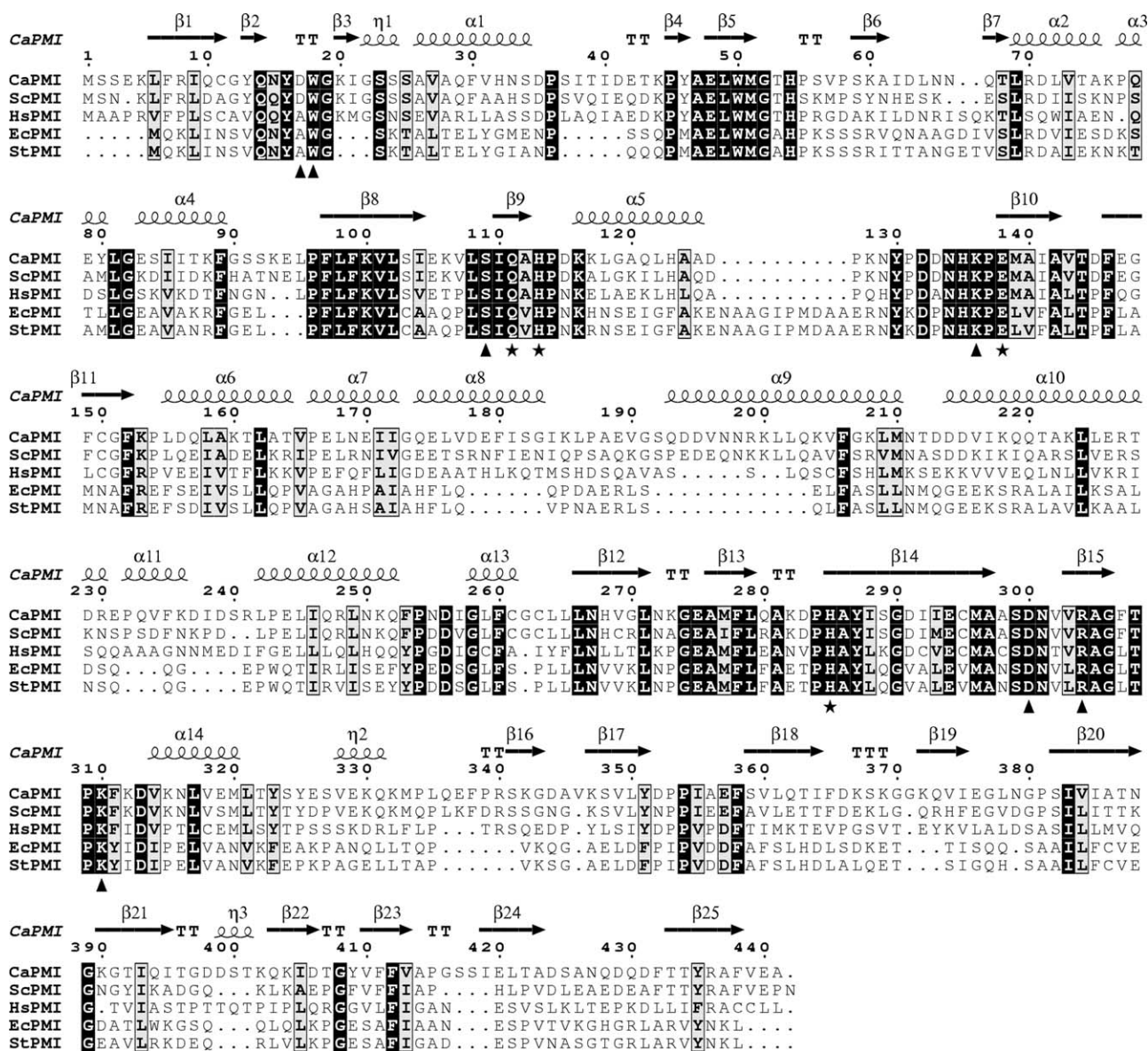


Figure 4

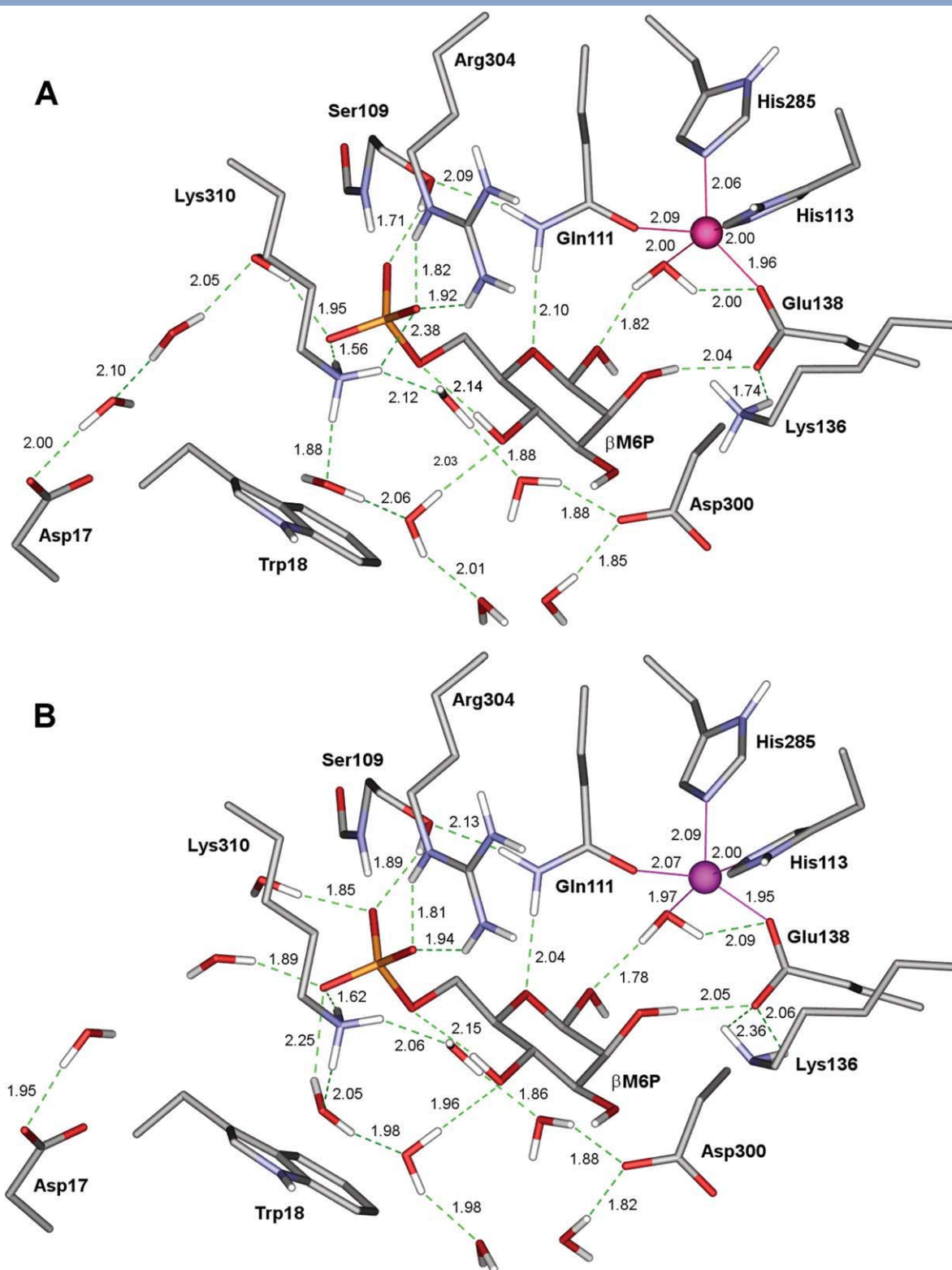
Amino acid sequence alignment of PMIs from *C. albicans*, *S. cerevisiae*, human, *E. coli*, and *S. typhimurium*. The sequence numbering and secondary structure assignment shown at the top correspond to CaPMI. The alignment length is 454 aa, with residues that are conserved in all sequences shown as white characters with a black background (84 residues, 18.50%). Residues that are similar in all sequences are shown as black characters with a gray background (42 residues, 9.25%). The zinc ligands are labeled with an asterisk at the bottom of the alignment. The other residues shown in the SIBFA modeling of the CaPMI active site are labeled with a triangle. This alignment was achieved with CLUSTALW⁶⁸ on NPS@ server⁶⁹ and was illustrated with ESPrnt (similarity calculations parameters used: type = % of equivalent residues; global score = 0.8).⁷⁰

ger inhibitor than 5PAHz, with K_m/K_i ratio values of 4100 and 160, respectively, both compounds can be considered to be good HEI analogue inhibitors of the M6P to F6P isomerization reaction catalyzed by EcPMI.

Sequence alignment

Results of the inhibition studies on HsPMI and EcPMI reported in Table I and comparison with those previously reported on ScPMI⁴⁵ clearly show that all Type I PMIs

studied behave relatively similarly. Even though Type I PMIs from *C. albicans*, *S. cerevisiae*, *H. sapiens*, *E. coli*, and *S. typhimurium* share only 19% amino acid sequence identity (28% identical or strongly similar), the active site amino acids are conserved (Fig. 4 and Supporting Information Fig. S2). More importantly, those active site residues in the theoretical model of CaPMI that interact (within 2.4 Å) with the zinc metal cofactor and the cyclic substrate β-M6P (Fig. 5) or the HEI analogue inhibitor 5PAH (Fig. 6) are 100% conserved. This observation sug-

**Figure 5**

Representation of the active sites of the lowest energy models of Type I PMI from *C. albicans* complexed with the cyclic substrate β -D-mannopyranose 6-phosphate (β -M6P) obtained through SIBFA computations, in which either a cationic (**A**) or a neutral (**B**) Lys136 side chain is considered respectively. The models show the zinc-bound water molecule and Gln111 postulated to be involved in ring-opening of the cyclic substrate. The zinc metal cofactor is depicted as a sphere, plain lines indicate coordinating bond interactions, and the dashed lines indicate hydrogen bond interactions. The lengths of potential hydrogen bonds and of coordinating bonds are shown (in Angströms) next to the dashed and plain lines, respectively. DS Visualizer 2.0,⁷¹ Pov-Ray 3.6,⁷² and Gimp 2.0⁷³ software were used to prepare the figure. [Color figure can be viewed in the online issue, which is available at wileyonlinelibrary.com.]

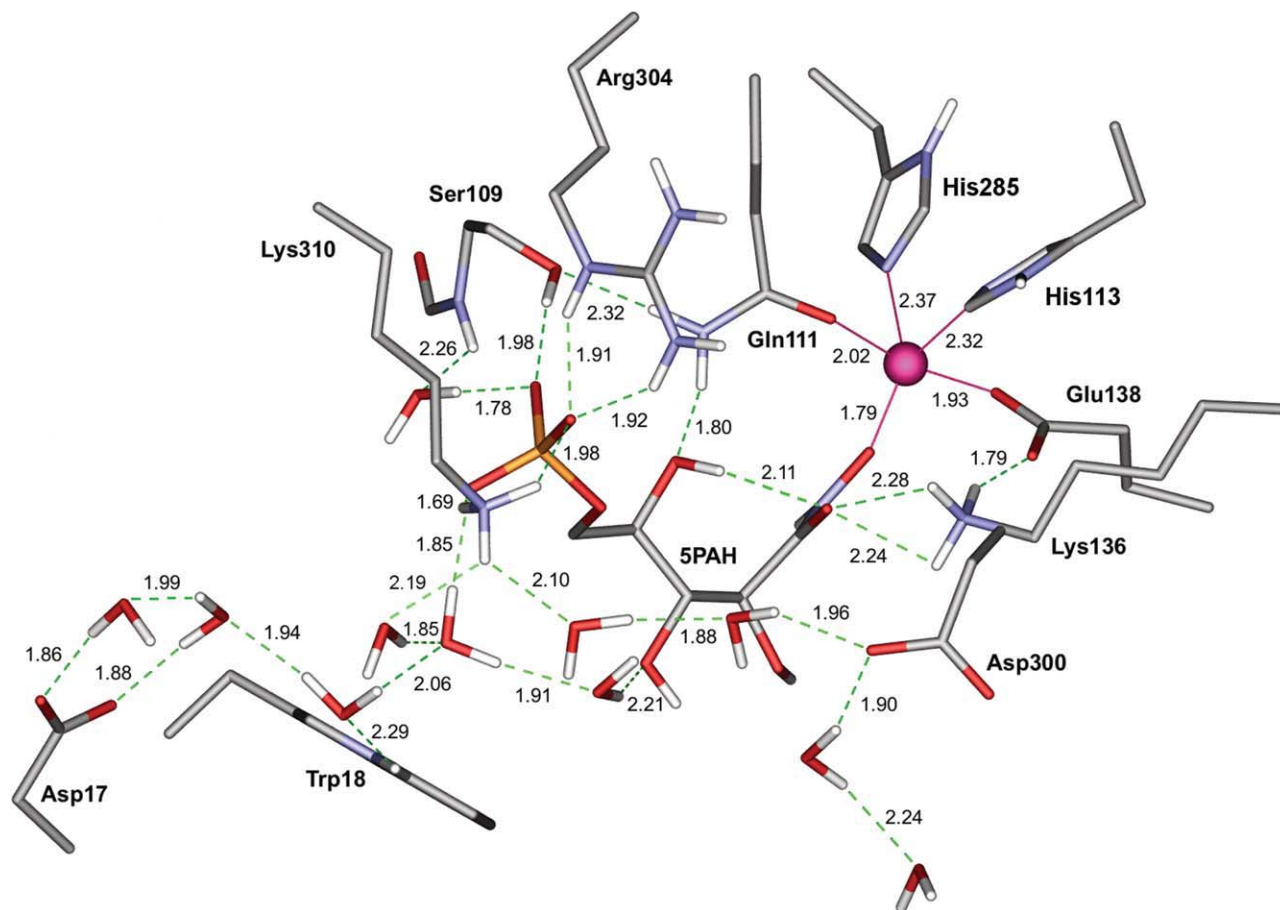


Figure 6

Representation of the active site of the lowest energy model of Type I PMI from *C. albicans* complexed with the HEI analogue inhibitor 5PAH obtained through SIBFA computations. The model shows Lys136 to be ideally situated for proton transfer between the C1 and C2 atoms of the corresponding linear substrate M6P or F6P. The zinc metal cofactor is depicted as a sphere, plain lines indicate coordinating bond interactions, and the dashed lines indicate hydrogen bond interactions. The lengths of potential hydrogen bonds and of coordinating bonds are shown (in Angströms) next to the dashed and plain lines, respectively. DS Visualizer 2.0,⁷¹ Pov-Ray 3.6,⁷² and Gimp 2.0⁷³ software were used to prepare the figure.

gests we can generalize the conclusions about mechanisms drawn from inhibition and molecular mechanics studies of CaPMI to the other Type I PMIs considered herein, and notably to human PMI.

β -M6P and 5PAH binding in the CaPMI active site

Besides the crystal structures of StPMI which were very recently reported by Sagurthi *et al.*,¹⁶ the crystal structure of CaPMI reported by Cleasby *et al.* (PDB ID code 1PMI) is one of the few PMI structures described in the literature.¹² Because we did not succeed in obtaining high-resolution crystal structures of PMI complexes, the polarizable molecular mechanics procedure SIBFA⁴⁶ was used here to analyze the structural and energetics aspects of β -M6P and 5PAH binding to a 164-residue model of CaPMI including an additional array of highly polarized discrete water molecules in the binding site. The SIBFA procedure was previously

applied successfully to study several inhibitor-metalloprotein complexes.^{25,44,47–50,53,74} We used the three-dimensional structure of the Type I *C. albicans* PMI¹² as a starting point to generate a theoretical model of the enzyme, and thereafter the different complexes of the model with the substrate or the inhibitor and the array of discrete water molecules.

The active sites of the lowest SIBFA energy-minimized representations of *C. albicans* PMI complexed with β -D-mannopyranose 6-phosphate (β -M6P), including a zinc-bound water molecule plus an array of nine water molecules, are depicted in Figure 5(A,B), in which either a cationic or a neutral Lys136 side chain is considered, respectively. In these similar energy-minimized structures, the zinc metal cofactor has a coordination number of five. The ligands are arranged around the metal ion as a distorted trigonal bipyramid. A water molecule is bound to Zn(II), which is also liganded by four side chain atoms from the protein, Gln111 O ϵ 1, His113 N ϵ 2, Glu138 O ϵ 1, and His285 N ϵ 2. A very similar zinc environment is found in the

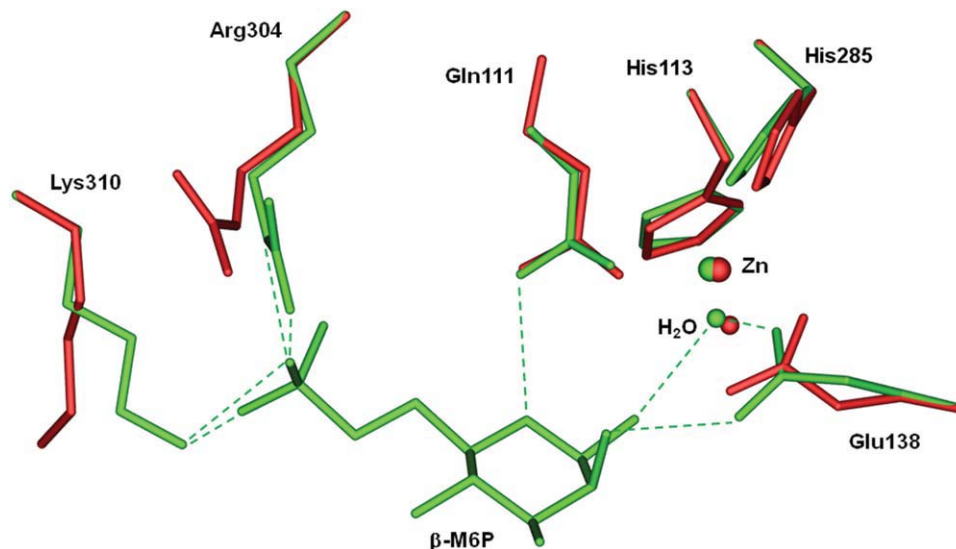


Figure 7

Structural alignment of the active site residues of the SIBFA-computed model structures of CaPMI complexed to β -M6P (green or light gray) and of the apoenzyme (red or dark gray). The zinc metal cofactor is depicted as a large sphere and the water molecule as a smaller sphere. The dashed lines indicate hydrogen bond interactions for the CaPMI- β -M6P energy-minimized structure. DS Visualizer 2.0,⁷¹ Pov-Ray 3.6,⁷² and Gimp 2.0⁷³ software were used to prepare the figure. [Color figure can be viewed in the online issue, which is available at wileyonlinelibrary.com.]

reported crystal structure of CaPMI.²² It is important in this respect that a correct pentacoordination of zinc was retained at the outcome of EM without enforcing any zinc ligand distances, as is the case with most classical force fields. The zinc-bound water molecule further forms two hydrogen bonds with the oxygen atoms of Glu138 and with the hydroxyl group on C1 of β -M6P. Glu138 forms additional H-bonds through its O ϵ 2 oxygen atom with Lys136 and the hydroxyl group on C2 of β -M6P. The O atom of the C3 hydroxyl has a weak H-bond ($dO-H = 2.7 \text{ \AA}$) with one H atom of the protonated Lys136 residue (Figure 5(A)). The O atom of the C4 hydroxyl is H-bonded to a water molecule. The ring oxygen atom on C5 of β -M6P is H-bonded to the NH₂ group of Gln111, a residue thus likely to be involved in the ring-opening step of β -M6P. The phosphoryl group of β -M6P forms hydrogen bonds to the side chains of Ser109, Arg304, Lys310, and a water molecule. The phosphate ester oxygen atom on C6 appears also intramolecularly H-bonded to the hydroxyl group on C4. Ser109 further interacts through its side chain O atom with the side chain amino group of Gln111, and Lys310 with two water molecules. The nine discrete water molecules are distributed in three arrays of three water molecules each: at the entrance of the binding pocket between Asp17 and the phosphate group of β -M6P, between Lys310 and Asp300, and between Lys310 and Glu48, the latter being part of a network involving successively Glu48, Lys100, Glu294, and Tyr287 (not shown). The overall energy-minimized structure depicted in Figure 5(A) is similar to the corresponding energy-minimized structure we reported without the array of discrete water molecules²⁵ except for the phosphoryl group of the

substrate and the amino side chain group of Lys310, which moved by 0.3 and 0.2 \AA , respectively. The similarity indicates the limited perturbation of the structures by the polarized discrete water molecules. On the other hand, they were found to play an essential role in the comparative energy balances of complexation of competing ligands (Gresh *et al.*, in preparation). However, superposition of the model with the structure of the apoenzyme (PDB code 1PMI) shows a rather significant displacement of Arg304 and Lys310 toward the phosphoryl group of the substrate upon binding of β -M6P to the enzyme active site (Fig. 7).

The active site of the SIBFA energy-minimized structure of *C. albicans* complexed with the anion hydroxamate 5PAH, including the array of 11 water molecules, is represented in Figure 6. It is noted that only a cationic Lys136 side chain is now considered. This could occur by proton abstraction from the 5PAH hydroxamic acid moiety which, having a pK_a of 9.6,⁴⁵ is predominantly in its acid form when uncomplexed in aqueous solution. Zn(II) is fivefold coordinated. The ligands are arranged around it at the apexes of a distorted trigonal bipyramid. The hydroxamate moiety of the inhibitor is bound in a monodentate mode to Zn(II) through its N-connected O atom. Zn(II) is also liganded by four side chain atoms from the protein, Gln111 O ϵ 1, His113 N ϵ 2, Glu138 O ϵ 1, and His285 N ϵ 2. A similar zinc environment is found in the reported crystal structure of CaPMI, excepted that a water molecule is found in place of the N-connected O atom of 5PAH.²² The carbonyl O atom on C1 of 5PAH (which corresponds to the O atom on C2 of the substrate) forms two hydrogen bonds to Lys136, a residue which appears to be a possible candidate for proton

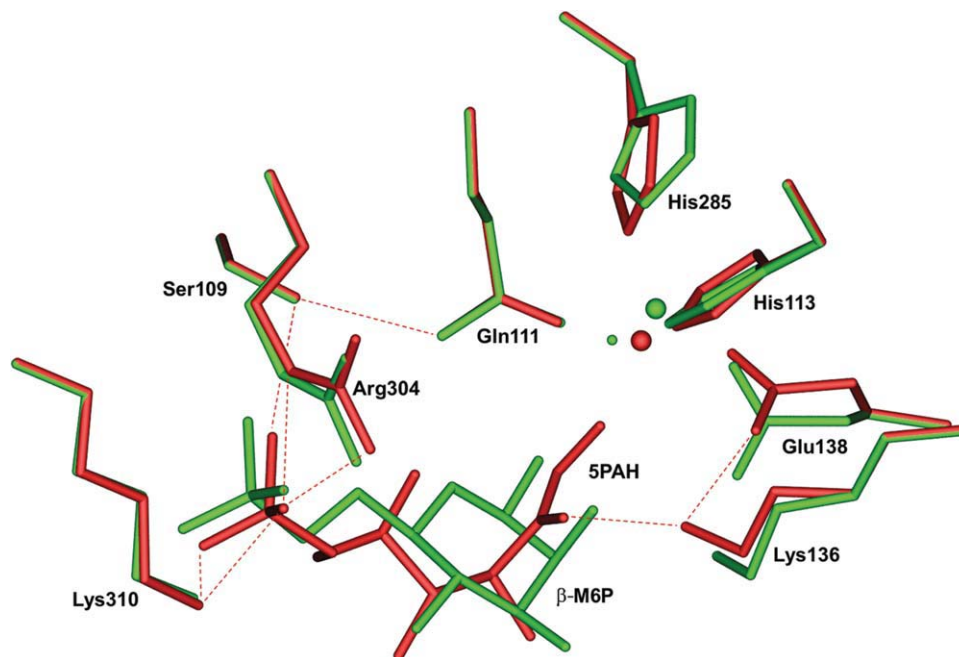


Figure 8

Structural alignment of the active site residues of the SIBFA-computed model structures of CaPMI complexed to β -M6P (green or light gray) and to 5PAH (red or dark gray). The zinc metal cofactor is depicted as a large sphere and the water molecule as a smaller sphere. The dashed lines indicate hydrogen bond interactions for the CaPMI-5PAH energy-minimized structure. DS Visualizer 2.0,⁷¹ Pov-Ray 3.6,⁷² and Gimp 2.0⁷³ software were used to prepare the figure. [Color figure can be viewed in the online issue, which is available at wileyonlinelibrary.com.]

transfer between the two carbon atoms C1 and C2 of the substrate M6P or F6P. Lys136 is also hydrogen bonded to Glu138 O ϵ 2. The distances from the Lys136 side-chain N atom to the C1 and N atoms of 5PAH are 3.4 and 3.8 Å, respectively. These are notably shorter than the corresponding distances from the Glu138 O ϵ 2 and O ϵ 1 atoms, which amount to 4.4 and 4.0 Å and to 4.9 and 4.0 Å, respectively. These structural data suggest that proton transfer should involve Lys136 rather than Glu138. This is supported by the pK_a values of these residues reported below. The phosphoryl group of 5PAH forms hydrogen bonds to the side chains of Ser109, Arg304, and Lys310, and a water molecule. The O atom on C4 of 5PAH interacts with the side chain amino group of Gln111. It should be noted that the latter O atom corresponds to the ring O atom on C5 of the substrate β -D-mannopyranose 6-phosphate (β -M6P) or β -D-fructofuranose 6-phosphate (β -F6P), which supports the model that Gln111 is a good candidate to be a catalytic residue involved in the potentially enzyme-catalyzed initial ring opening step. The hydroxyl group on C4 of the inhibitor could also be intramolecularly hydrogen bonded to the O atom on C1. Ser109 further interacts through its side chain O atom with the side chain amino group of Gln111. Ten of 11 discrete water molecules are part of an array of hydrogen bonds involving Asp17, Trp18, Lys310, Asp300, and His54 (not shown) in the vicinity of the hydroxyl groups on C2 and C3 and of the phosphoryl group of 5PAH. The other water

molecule forms hydrogen bonds with the backbone NH group of Ser109 and the phosphoryl group of 5PAH. The oxygen atom of the hydroxyl group on C3 of 5PAH is H-bonded to a water molecule. Although no strong interactions could be detected for the hydroxyl group on C2 with active site residues or water molecules, it could be weakly hydrogen bonded to Lys100, a residue being part of a network involving successively Glu48, Lys100, Glu294, and Tyr287 (not shown). Superimposition with the SIBFA energy-minimized structure of CaPMI complexed to β -M6P shows a significant move of the O1 oxygen atom of the ligand toward the zinc metal cofactor, as well as of the zinc metal cofactor itself (0.7 Å), His113 and Lys136 toward the ligand. These movements result from the strong interactions of the substrate in a high-energy intermediate form, as mimicked by 5PAH, with PMI along with the removal of the Zn(II)-bound water molecule (Fig. 8).

DISCUSSION

In this study, we report the kinetic evaluation of two HEI analogue inhibitors, 5PAH and 5PAHz, on two Type I PMIs: commercially available EcPMI and recombinant HsPMI, which was overexpressed and purified through a much more efficient procedure than previously reported.⁴ This improved procedure allowed us to obtain

large amounts of HsPMI for studies of its kinetics and inhibition studies. It may also facilitate structure-activity studies, in particular through X-ray crystallography, although our attempts to grow crystals did not lead to successful results yet.

As we reported before for the Type I ScPMI and Type II PaPMI catalyzed isomerisation reactions of M6P to F6P,⁴⁵ 5PAH is also the strongest competitive inhibitor ever evaluated for both Type I HsPMI and bacterial EcPMI. Whatever PMI is considered, the high K_m/K_i ratio values we determined (Table I) suggest a much stronger structural analogy of the inhibitor with the reaction HEI than with the substrate M6P or F6P. In addition, it is interesting to note that we report higher K_m/K_i ratio values for bacterial PMIs from *E. coli* and *P. aeruginosa*, 4100 and 18,250,⁴⁵ respectively, than for eukaryotic enzymes from yeast and human, 1410⁴⁵ and 1000, respectively. Although the ratio is only slightly larger for the bacterial over the eukaryotic enzymes, which indicates a rather high degree of homology of the active site of PMIs whatever type or source is considered, these results for 5PAH are encouraging for the future development of molecules of therapeutic interest targeting bacterial PMIs.

Comparison of the K_i values of 5PAH and 5PAHz on both human and *E. coli* PMIs reported in Table I shows that 5PAHz is much less efficient than 5PAH as an inhibitor of the enzyme catalyzed isomerization of M6P to F6P (Table I). The ratio $K_i(5PAH)/K_i(5PAHz)$ is in the range of 20, which corresponds to a 1.8 kcal mol⁻¹ increase in the binding affinity of 5PAH versus 5PAHz for the enzyme active site. The pK_a value of 5PAHz is not available, but hydrazides are known to have such values above 15, as compared with 5PAH for which we reported a pK_a value of 9.6.⁴⁵ Consequently, 5PAHz is neutral in solution and most likely at the enzyme active site, whereas 5PAH is partly anionic in solution and most likely anionic at the enzyme active site, that is, in its hydroxamate or hydroximate form as we previously proposed for the PGI catalyzed reversible isomerization of G6P and F6P.⁵⁸ It seems likely that electrostatic stabilization of a 1,2-*cis*-enediolate HEI plays a significant role in the catalytic mechanism of PMI, a hypothesis also formulated in the case of the TIM catalyzed reversible isomerization of dihydroxyacetone phosphate and glyceraldehyde 3-phosphate.³³ In the case of Type I PMIs, the anionic nature of the HEI is further supported by the Lewis acid character of the enzyme active site zinc cofactor and the nearby cationic residue Lys136-NH₃⁺.

In an attempt to propose an overall mechanism for the M6P to F6P reversible isomerization catalyzed by Type I PMIs, we should first consider the question of whether the enzyme active site binds the cyclic or linear form of the substrate M6P. To date, no crystal structure of a PMI-M6P complex is available to answer this question. However, based on the following observations, we

propose the hypothesis that the enzyme active site recognizes the cyclic form of the substrate preferentially to its linear form. First, PMIs use a sugar substrate that exists in solution overwhelmingly in the hemiacetal ring form. To our knowledge, the amount of M6P present in solution in the open-chain form is not available, but a value for the free aldehyde form of mannose in solution is estimated to be about 0.064%.⁷⁵ Phosphorylated sugars are known to mutarotate faster than the corresponding non-phosphorylated sugars, so it has been assumed that about 50 times as much open chain form of the phosphorylated hexoses could be present in solution than of the free sugars.³⁶ In our hands, ¹³C NMR analysis of M6P in D₂O did not detect any of the linear form. Hence, considering that probably much less than 3% of the M6P present in aqueous solution is linear, it is difficult to conceive, from an efficiency point of view, that the enzyme will exclusively use this minor form. Second, the α anomer of D-mannopyranose 6-phosphate (α -M6P) is a weak inhibitor of the enzyme, whereas the β anomer (β -M6P) is a substrate.² Thus, if the linear form of M6P were the only form of the substrate to bind to the enzyme active site, both α -M6P and β -M6P would behave similarly. Third, we also investigated the SIBFA energy-minimized structures of CaPMI complexed to the cyclic α -M6P and linear M6P (data not shown). The energy balances resulted in a significant preference favoring the complex of β -M6P isomer with CaPMI (Fig. 5) over that of the α -M6P isomer (work in preparation). Consequently, it seems reasonable to propose that the true M6P substrate of PMIs is the cyclic substrate β -M6P. Because the substrate must be in the open-chain form for proton transfer to occur between C1 and C2, the above hypothesis implies that the enzyme catalyzes a second activity, that of ring-opening, before the isomerization step itself. Comparison to other aldose-ketose isomerases like xylose isomerase,^{29,31} phosphoglucose isomerase,⁷⁶⁻⁷⁸ and phosphoribose isomerase,⁷⁹ for which an enzyme-catalyzed ring-opening step of the corresponding substrate has been demonstrated, is also in accord with a similar PMI-catalyzed primary step with the cyclic substrate β -M6P or β -F6P.

As we previously reported, initial binding of the cyclic substrate β -M6P does not imply displacement of the zinc-bound water molecule observed in the crystal structure of the free enzyme reported by Cleasby *et al.*¹² However, a significant displacement of two cationic residues of the binding pocket, namely Lys310 and Arg304, is observed upon binding of the substrate in a classical induced-fit mechanism (Fig. 7). The substrate β -M6P is thus strongly stabilized at the binding site of CaPMI through interaction of its phosphoryl group with residues located at the entrance of the binding cleft including Ser109, Lys310, and Arg304, as well as a water molecule. For reasons unclear to us, Sagurthi *et al.* also reported binding of the cyclic substrate β -F6P to StPMI, also a

Type I PMI, in a different binding site which notably does not involve Arg304.¹⁶ However, Arg304 was firmly identified as a residue of the active site of CaPMI by enzyme inactivation using phenylglyoxal in absence of substrate. On the contrary, coincubation of the enzyme with substrate was reported to protect the enzyme from this inactivation, suggesting a direct interaction of Arg304 with the substrate.¹³ Furthermore, the reported structure of Type I phosphate-bound *B. subtilis* PMI clearly shows interaction of inorganic phosphate with Arg193, the residue equivalent to Arg304 in CaPMI.⁴¹ We have attempted to perform new energy-minimizations of CaPMI complexed with β -M6P in the binding site identified for β -F6P on the StPMI structure.¹⁶ We tried using SIBFA as well as the Accelrys CFF91⁸⁰ classical force-field. Severe steric clashes were invariably encountered, which prevented us from obtaining any meaningful structure. The models represented in Figure 5 also show the highly conserved Gln111 binding through its side-chain amide group to the O5 ring oxygen atom of the substrate β -M6P. Hence, we propose that Gln111 is involved in the enzyme-catalyzed ring-opening step through interaction of its amide side-chain group with the oxygen atom of the pyranose ring of the cyclic substrate. Gln111 would thus facilitate ring-opening of the substrate with the assistance of the zinc-bound water molecule. Following ring-opening, a change in the conformation of M6P would allow the oxygen atom on C1 to displace the zinc-bound water molecule so that the C1—C2 part of the substrate is in a position suitable for the second enzyme activity, isomerization, to take place.

The mechanism of the isomerization step could be described based on the model of a detailed view of the HEI analogue inhibitor (5PAH) complexed to the active site zinc of the Type I PMI from *C. albicans* (Fig. 6). All the active site residues of Type I PMIs mentioned in this study are conserved, as shown by the sequence alignment in Figure 4. The lowest SIBFA energy-minimized structure obtained for the CaPMI-5PAH complex clearly shows the hydroxamate inhibitor bound in a monodentate mode to the zinc cofactor. This model first highlights the importance of the hydroxyl groups of C2 and C4 of 5PAH which correspond to C3 and C5 of the substrate. These hydroxyls are in the vicinity of Lys100 and Gln111, respectively. The only hydroxyl group not engaged in hydrogen bonding with an active site residue is the one on C3 of 5PAH, corresponding to C4 of the substrate M6P. It is nevertheless bound to a water molecule itself interacting, through three other water molecules, with the conserved Trp18. This observation suggests that modification of the inhibitor at this position could be envisioned to increase the inhibition efficiency and species selectivity. A neutral Lys136 appears as the best candidate for the active site catalytic base of Type I PMIs thought to be involved in the proton transfer between C1 and C2 of the substrates. As shown in Figure 6, Lys136 is the

closest residue to the N and C1 atoms of 5PAH, which correspond to the C1 and C2 carbon atoms of the substrate, respectively. Within the class of aldose-ketose isomerases, however, identifying a lysine residue as the probable catalytic base involved in the proton transfer between the two adjacent carbons of the substrates catalyzed by Type I PMIs is unique. Indeed, except in the case of aldose-ketose isomerases that proceed through a hydride shift mechanism, like xylose isomerase, a glutamate residue has always been identified as the catalytic base for aldose-ketose isomerases that proceed through a proton transfer mechanism like triosephosphate isomerase and phosphoglucose isomerase.

Because of its strong interaction with the zinc cation and Lys136, Glu138 displays a PROPKA^{81,82} calculated pK_a value of -7.0 ± 0.9 , which indeed makes this residue very unlikely to act as a base in the ring opening step of the substrate, nor in the proton transfer between C1 and C2 of the substrate. Consequently, ring-opening of the substrate at the active site might indeed occur in a concerted manner with the assistance of the zinc-bound water molecule and Gln111. Interestingly, the calculated pK_a value for Lys136 with PROPKA gives 7.6 ± 0.9 , which is about three pK_a units below the value in aqueous solution. Lys136 could thus be easily deprotonated at physiological pH or at pH of PMI activity (range 6.5–8) or can even be nonprotonated. Indeed, we have performed a SIBFA modeling study of the enzyme-substrate complex with a neutral Lys136 [Fig. 5(B)] that shows no differences when compared with the complex with a protonated Lys136 [Fig. 5(A)]. Lys136 is too far from the anomeric OH group of the substrate and from the zinc-bound water molecule to be involved in the ring-opening of the substrate. On the other hand, a neutral Lys136-NH₂ residue is likely to be involved in proton transfer between the C1 and C2 carbon atoms of the substrate. This step would involve the 1,2-*cis*-enediolate HEI and a protonated Lys136, as mimicked by our model depicted in Figure 6 of CaPMI complexed with the anion hydroxamate 5PAH. It should be added that Gracy and Noltmann reported that, from the pH dependence of the kinetic parameters, pK_a values of 6.6 and 7.8 for the free enzyme and of 6.4 and 8.1 for the enzyme-substrate complex had been determined for two ionizable groups involved in substrate binding and catalysis. The pK_a values of 6.6 and 6.4 had been attributed to a histidine residue, but this seems very unlikely considering that the PROPKA calculated values for the two His active site residues, namely His113 and His285, are -1.5 and -0.8 , respectively. The second pK_a value corresponds to the calculated Lys136 pK_a of 7.6 ± 0.9 .

In view of our results, the proposed multistep mechanism of the M6P to F6P reversible isomerization reaction catalyzed by Type I PMIs is depicted in Figure 9 and is detailed below. The numbering of the steps refers to the M6P to F6P direction of catalysis. The consideration of a

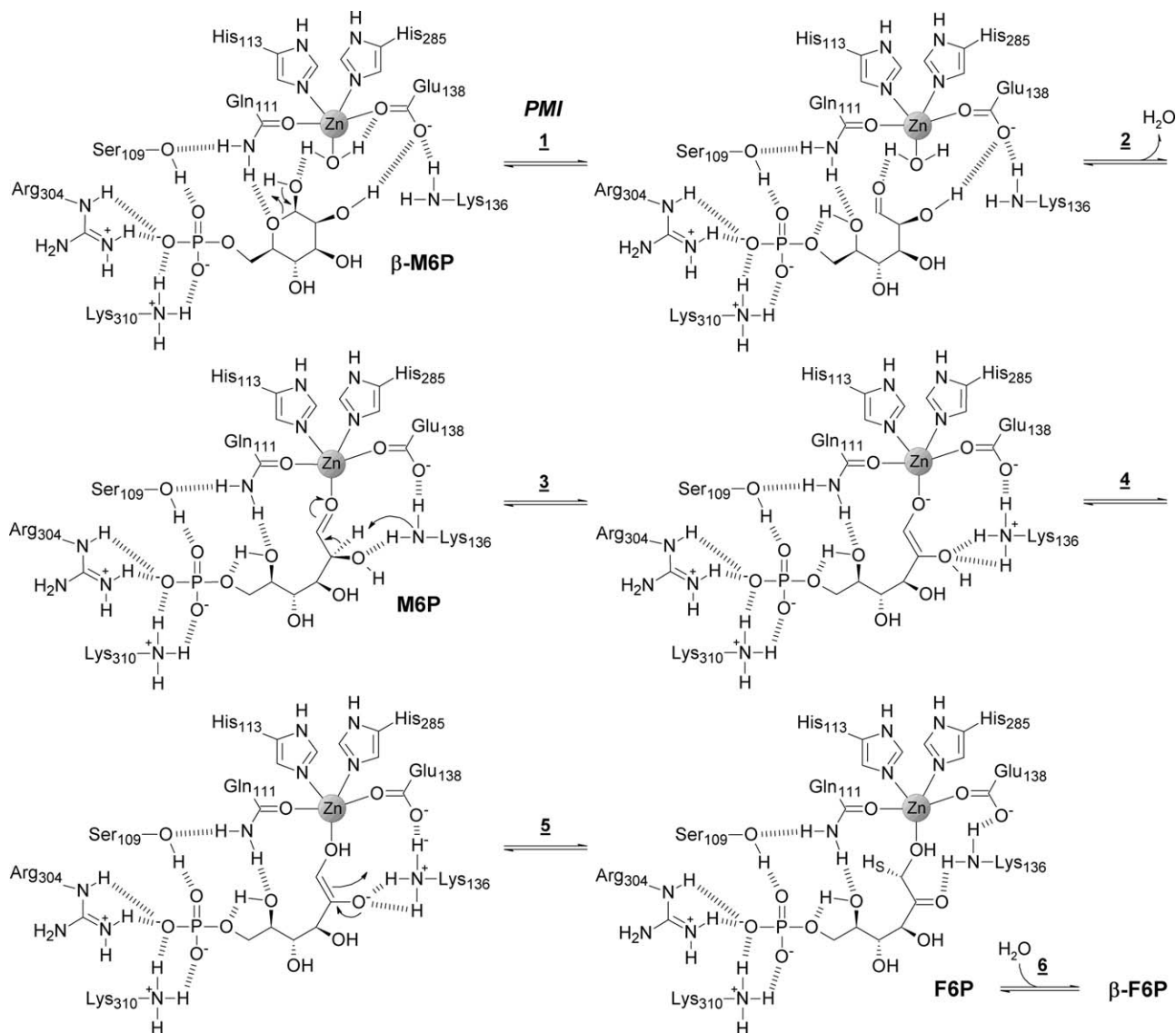


Figure 9

The proposed multistep mechanism of the M6P to F6P reversible isomerization reaction catalyzed by Type I PMIs (the numbering of the steps refers to the M6P to F6P direction of catalysis). (1) Ligand binding and ring opening: Assisted by the zinc-bound water molecule and Gln111, displacement of electrons and proton transfer between the oxygen atoms O1 and O5 induce cleavage of the C1—O5 bond and generate the open form of M6P. (2) Conformational change and water displacement: following displacement of the zinc-bound water molecule, zinc coordination of the O1 oxygen atom of M6P allows favorable interaction of its hydroxyl group on C2 with the nearby Lys136. (3) Isomerization: the neutral Lys136-NH₂ residue thereafter abstracts the hydrogen on C2 of M6P to yield the first 1,2-*cis*-enediolate HEI stabilized through interaction with Zn²⁺ and Lys136-NH₃⁺. (4) Proton transfer: proton transfer between O1 and O2 yields the second 1,2-*cis*-enediolate HEI. (5) Product formation: linear F6P is formed by protonation of the C1 carbon atom of the HEI on its *Si* face by Lys136-NH₃⁺, yielding Lys136-NH₂. (6) Ring closure and product release: upon entry of a new water molecule and cyclization, β -D-fructofuranose 6-phosphate (β -F6P) is released from the active site upon binding of β -M6P. ACD/Chemsketch software was used to prepare the figure.⁸³

neutral Lys136 residue is justified by its calculated pK_a value, implying a stabilization of the neutral form possibly coexisting with the cationic one. It is also consistent with the result by Gracy and Noltmann. Figure 5(A,B) also show that in their complexes with β -M6P, the side chains of the cationic and of the neutral Lys136 residue occupy similar positions. (1) Ligand binding and ring opening: the cyclic substrate β -D-mannopyranose 6-phosphate (β -

M6P) binds to the zinc-bound water molecule through its O1 oxygen atom and to Glu138 through its C2 hydroxyl group, to Gln111 through its ring O5 oxygen atom, and to Ser109, Arg304, and Lys310 through its phosphoryl group. In a probably concerted mechanism, and with the favorable assistance of Gln111 and the zinc-bound water molecule, displacement of electrons and proton transfer between the oxygen atoms O1 and O5 induce cleavage of the

C1—O5 bond and generate the open form of M6P. (2) Conformational change and water displacement: following displacement of the zinc-bound water molecule, zinc coordination of the O1 oxygen atom of M6P allows favorable interaction of its hydroxyl group on C2 with the nearby Lys136. (3) Isomerization: the neutral Lys136-NH₂ thereafter abstracts the hydrogen on C2 of M6P to yield the first 1,2-*cis*-enediolate HEI stabilized through interaction with Zn²⁺ and Lys136-NH₃⁺. (4) Protontropy: proton transfer between O1 and O2 yields the second 1,2-*cis*-enediolate HEI also stabilized through interaction with the metal cofactor and Lys136-NH₃⁺. (5) Product formation: linear F6P is formed by protonation of the C1 carbon atom of the HEI on its *Si* face by Lys136-NH₃⁺, yielding Lys136-NH₂. (6) Ring closure and product release: upon entry of a new water molecule and cyclization, β-D-fructofuranose 6-phosphate (β-F6P) is released from the active site upon binding of β-M6P.

In conclusion, our inhibition and theoretical studies of Type I PMIs reported here allowed us to identify the active site residues and to propose a role for each of them in the enzyme catalyzed reversible ring-opening and isomerization reactions of β-M6P to β-F6P. We are aware that some parts of the mechanism, which are based on relative movements (or distances) between residues and substrate, lack the required dynamic information. However, as far as we know, molecular dynamics on metalloproteins is not possible at the present time, although it is currently a subject under study in our group with SIBFA.

REFERENCES

- Jensen SO, Reeves PR. Domain organisation in phosphomannose isomerase (types I and II). *Biochem Biophys Acta* 1998; 1382:5–7.
- Malaisse-Lagae F, Liemans V, Yaylali B, Sener A, Malaisse WJ. Phosphoglucosomerase-catalysed interconversion of hexose phosphates; comparison with phosphomannoisomerase. *Biochim Biophys Acta* 1989;998:118–125.
- Rose IA, O'Connell EL, Schray KJ. Mannose 6-phosphate: anomeric form used by phosphomannose isomerase and its 1-epimerization by phosphoglucose isomerase. *J Biol Chem* 1973;248: 2232–2234.
- Proudfoot AEI, Turcatti G, Wells TNC, Payton MA, Smith DJ. Purification, cDNA cloning and heterologous expression of human phosphomannose isomerase. *Eur J Biochem* 1994;219:415–423.
- Swan MK, Hansen T, Schönheit P, Davies C. A novel phosphoglucose/phosphomannose isomerase from *Pyrobaculum aerophilum* is a member of the PGI superfamily: structural evidence at 1.16 Å resolution. *J Biol Chem* 2004;279:39838–39845.
- Swan MK, Hansen T, Schönheit P, Davies C. Structural basis for phosphomannose isomerase activity in phosphoglucose isomerase from *Pyrobaculum aerophilum*: a subtle difference between distantly related enzymes. *Biochemistry* 2004;43:14088–14095.
- Gracy RW, Noltmann EA. Studies on phosphomannose isomerase I. Isolation, homogeneity measurements, and determination of some physical properties. *J Biol Chem* 1968;243:3161–3168.
- Proudfoot AEI, Payton MA, Wells TNC. Purification and characterization of fungal and mammalian phosphomannose isomerases. *J Protein Chem* 1994;13:619–627.
- Wells TNC, Payton MA, Proudfoot AEI. Phosphomannose isomerase from *Saccharomyces cerevisiae* contains two inhibitory metal ion binding site. *Biochemistry* 1993;32:1294–1301.
- Pitkänen J, Törmä A, Alff S, Huopaniemi SPM, Renkonen R. Excess mannose limits the growth of phosphomannose isomerase *PMI40* deletion strain of *Saccharomyces cerevisiae*. *J Biol Chem* 2004;279:55737–55743.
- Coulin F, Magnenat E, Proudfoot AEI, Payton MA, Scully P, Wells TNC. Identification of Cys-150 in the active site of phosphomannose isomerase from *Candida albicans*. *Biochemistry* 1993;32:14139–14144.
- Cleasby A, Wonacott A, Skarzynski T, Hubbard RE, Davies GJ, Proudfoot AEI, Bernard AR, Payton MA, Wells TNC. The X-ray crystal structure of phosphomannose isomerase from *Candida albicans* at 1.7 Å resolution. *Nat Struct Biol* 1996;3:470–479.
- Wells TNC, Scully P, Magnenat E. Arginine 304 is an active site residue in phosphomannose isomerase from *Candida albicans*. *Biochemistry* 1994;33:5777–5782.
- Smith JJ, Thomson AJ, Proudfoot AEI, Wells TNC. Identification of an Fe(III)-dihydroxyphenylalanine site in recombinant phosphomannose isomerase from *Candida albicans*. *Eur J Biochem* 1997;244:325–333.
- Miles JS, Guest JR. Nucleotide sequence and transcriptional start point of the phosphomannose isomerase gene (*manA*) of *Escherichia coli*. *Gene* 1991;32:41–48.
- Sagurthi SR, Gowda G, Savithri HS, Murthy MRN. Structures of mannose-6-phosphate isomerase from *Salmonella typhimurium* bound to metal atoms and substrate: implications for catalytic mechanism. *Acta Crystallogr Sect D* 2009;65:724–732.
- Wu B, Zhang Y, Zheng R, Guo C, Wang PG. Bifunctional phosphomannose isomerase/GDP-D-mannose pyrophosphorylase is the point of control for GDP-D-mannose biosynthesis in *Helicobacter pylori*. *FEBS Lett* 2002;519:87–92.
- Patterson JH, Waller RE, Jeevarajah D, Billman-Jacobe H, McConville MJ. Mannose metabolism is required for mycobacterial growth. *Biochem J* 2003;372:77–86.
- Shinabarger D, Berry A, May TB, Rothmel R, Fialho A, Chakrabarty AM. Purification and characterization of phosphomannose isomerase-guanosine diphospho-D-mannose pyrophosphorylase. *J Biol Chem* 1991;266:2080–2088.
- Garami A, Ilg T. The role of the phosphomannose isomerase in *Leishmania mexicana* glycoconjugate synthesis and virulence. *J Biol Chem* 2001;276:6566–6575.
- Payton MA, Rheinneck M, Klig LS, DeTiani M, Bowden E. A novel *Saccharomyces cerevisiae* secretory mutant possesses a thermolabile phosphomannose isomerase. *J Bacteriol* 1991;173:2006–2010.
- Smith DJ, Proudfoot AEI, De Tiani M, Wells TNC, Payton MA. Cloning and heterologous expression of the *Candida albicans* gene *PMI 1* encoding phosphomannose isomerase. *Yeast* 1995;11:301–310.
- Wills EA, Roberts IS, Del Poeta M, Rivera J, Casadevall A, Cox GM, Perfect J. Identification and characterization of the *Cryptococcus neoformans* phosphomannose isomerase-encoding gene, *MAN1*, and its impact on pathogenicity. *Mol Microbiol* 2001; 40:610–620.
- Smith DJ, Payton MA. Hyphal tip extension in *Aspergillus nidulans* requires the *manA* gene, which encodes phosphomannose isomerase. *Mol Cell Biol* 1994;14:6030–6038.
- Foret J, de Courcy B, Gresh N, Piquemal J, Salmon L. Synthesis and evaluation of non-hydrolyzable D-mannose 6-phosphate surrogates reveal 6-deoxy-6-dicarboxymethyl-D-mannose as a new strong inhibitor of phosphomannose isomerases. *Bioorg Med Chem* 2009;17:7100–7107.
- Xiao J, Guo Z, Guo Y, Chu F, Sun P. Computational study of human phosphomannose isomerase: insights from homology modeling and molecular dynamics simulation of enzyme bound substrate. *J Mol Graph Model* 2006;25:289–295.

27. Whitlow M, Howard AJ, Finzel BC, Poulos TL, Winborne E, Gilliland GL. A metal-mediated hydride shift mechanism for xylose isomerase based on the 1.6 Å *Streptomyces rubiginosus* with xylitol and D-xylose. *Proteins* 1991;9:153–173.
28. Allen KN, Lavie A, Farber GK, Glasfeld A, Petsko GA, Ringe D. Isotopic exchange plus substrate and inhibition kinetics of D-xylose isomerase do not support a proton-transfer mechanism. *Biochemistry* 1994;33:1481–1487.
29. Allen KN, Lavie A, Glasfeld A, Tanada TN, Gerrity DP, Carlson SC, Farber GK, Petsko GA, Ringe D. Role of the divalent metal ion in sugar binding, ring opening, and isomerization by D-xylose isomerase: replacement of a catalytic metal by an amino acid. *Biochemistry* 1994;33:1488–1494.
30. Allen KN, Lavie A, Petsko GA, Ringe D. Design, synthesis and characterization of a potent xylose isomerase inhibitor, D-threonyhydroxamic acid, and high-resolution X-ray crystallographic structure of the enzyme-inhibitor complex. *Biochemistry* 1995;34:3742–3749.
31. Fenn TD, Ringe D, Petsko GA. Xylose isomerase in substrate and inhibitor michaelis states: atomic resolution studies of a metal-mediated hydride shift. *Biochemistry* 2004;43:6464–6474.
32. Korndörfer IP, Fessner WD, Matthews BW. The structure of rhamnose isomerase from *Escherichia coli* and its relation with xylose isomerase illustrates a change between inter and intra-subunit complementation during evolution. *J Mol Biol* 2000;300:917–933.
33. Davenport RC, Bash PA, Seaton BA, Karplus M, Petsko GA, Ringe D. Structure of the triosephosphate isomerase-phosphoglycolhydroxamate complex: an analogue of the intermediate on the reaction pathway. *Biochemistry* 1991;30:5821–5826.
34. Rose I, O'Connell E. Intramolecular hydrogen transfer in the phosphoglucose isomerase. *J Biol Chem* 1961;236:3086–3092.
35. Topper YJ. On the mechanism of action of phosphoglucose isomerase and phosphomannose isomerase. *J Biol Chem* 1957;225:419–425.
36. Gracy RW, Noltmann EA. Studies on phosphomannose isomerase. III. A mechanism for catalysis and for the role of zinc in the enzymatic and the nonenzymatic isomerization. *J Biol Chem* 1968;243:5410–5419.
37. Gracy R, Noltmann E. Studies on phosphomannose isomerase. II. Characterization as a zinc metalloenzyme. *J Biol Chem* 1968;243:4109–4116.
38. Noltmann EA. Aldose-ketose isomerases. In: Boyer PD, editor. *The enzymes*, Vol. 3. New York: Academic Press; 1972. pp 271–354.
39. Bentley R. Configurational and conformational aspects of carbohydrate biochemistry. *Annu Rev Biochem* 1972;41:953–996.
40. Berrisford JM, Hounslow AM, Akerboom J, Hagen WR, Brouns SJJ, van der Oost J, Murray IA, Blackburn GM, Waltho JP, Rice DW, Baker PJ. Evidence supporting a *cis*-enediol-based mechanism for *Pyrococcus furiosus* phosphoglucose isomerase. *J Mol Biol* 2006;358:1353–1366.
41. Kim Y, Lezondra L, Joachimiak A. Crystal structure analysis of the mannose-6-phosphate isomerase from *Bacillus subtilis*, DOI: 10.2210/pdb1qwr/pdb 2004.
42. Patskovsky Y, Ramagopal U, Toro R, Sauder JM, Iizuka M, Dickey M, Maletic M, Wasserman SR, Koss J, Burley SK, Almo SC. Crystal structure of mannose-6-phosphate isomerase from *Helicobacter pylori*, DOI: 10.2210/pdb2qh5/pdb 2007.
43. Cuff ME, Skarina T, Edwards A, Savchenko A, Joachimiak A. The structure of a putative mannosephosphate isomerase from *Archaeoglobus fulgidus*, DOI: 10.2210/pdb1zx5/pdb 2005.
44. Roux C, Gresh N, Perera LE, Piquemal J, Salmon L. Binding of 5-phospho-D-arabinonohydroxamate and 5-phospho-D-arabinonate inhibitors to zinc phosphomannose isomerase from *Candida albicans* studied by polarizable molecular mechanics and quantum mechanics. *J Comput Chem* 2007;28:938–957.
45. Roux C, Lee JH, Jeffery CJ, Salmon L. Inhibition of type I and type II phosphomannose isomerases by the reaction intermediate analogue 5-phospho-D-arabinonohydroxamic acid supports a catalytic role for the metal cofactor. *Biochemistry* 2004;43:2926–2934.
46. Gresh N, Cisneros GA, Darden TA, Piquemal J. Anisotropic, polarizable molecular mechanics studies of inter- and intramolecular interactions and ligand–macromolecule complexes. A bottom-up strategy. *J Chem Theory Comput* 2007;3:1960–1986.
47. Gresh N, Roques B. Thermolysin-inhibitor binding: effect of the His231 Ala mutation on the relative affinities of thiolate versus phosphoramidate inhibitors—a model theoretical investigation incorporating a continuum reaction field hydration model. *Biopolymers* 1997;41:145–164.
48. Garmer DR, Gresh N, Roques B. Modeling of inhibitor-metalloenzyme interactions and selectivity using molecular mechanics grounded in quantum chemistry. *Proteins* 1998;31:42–60.
49. Antony J, Gresh N, Olsen L, Hemmingsen L, Schofield C, Bauer R. Binding of D- and L-captopril inhibitors to metallo-beta-lactamase studied by polarizable molecular mechanics and quantum mechanics. *J Comput Chem* 2002;23:1281–1296.
50. Antony J, Piquemal J, Gresh N. Complexes of thiomandelate and captopril mercaptocarboxylate inhibitors to metallo-lactamase by polarizable molecular mechanics. Validation on model binding sites by quantum chemistry. *J Comput Chem* 2005;26:1131–1147.
51. Gresh N, Shi GB. Conformation-dependent intermolecular interaction energies of the triphosphate anion with divalent metal cations. Application to the ATP-binding site of a binuclear bacterial enzyme. A parallel quantum chemical and polarizable molecular mechanics investigation. *J Comput Chem* 2004;25:160–168.
52. Gresh N, Sponer JE. Complexes of pentahydrated Zn²⁺ with guanine, adenine, and the guanine-cytosine and adenine-thymine base pairs. Structures and energies characterized by polarizable molecular mechanics and *ab initio* calculations. *J Phys Chem B* 1999;103:11415–11427.
53. Gresh N, Derreumaux P. Generating conformations for two zinc-binding sites of HIV-1 nucleocapsid protein from random conformations by a hierarchical procedure and polarizable force field. *J Phys Chem B* 2003;107:4862–4870.
54. Gresh N, Sponer JE, Spacková N, Leszczynski J, Sponer J. Theoretical study of binding of hydrated Zn(II) and Mg(II) cations to 5'-guanosine monophosphate. Toward polarizable molecular mechanics for DNA and RNA. *J Phys Chem B* 2003;107:8669–8681.
55. Gresh N, Piquemal J, Krauss M. Representation of Zn(II) complexes in polarizable molecular mechanics. Further refinements of the electrostatic and short-range contributions. Comparisons with parallel *ab initio* computations. *J Comput Chem* 2005;26:1113–1130.
56. de Courcy B, Pedersen LG, Parisel O, Gresh N, Silvi B, Pilmé J, Piquemal J. Understanding selectivity of hard and soft metal cations within biological systems using the subvalence concept. 1. Application to blood coagulation: direct cation–protein electronic effects versus indirect interactions through water networks. *J Chem Theory Comput* 2010;6:1048–1063.
57. de Courcy B, Piquemal J, Garbay C, Gresh N. Polarizable water molecules in ligand–macromolecule recognition. Impact on the relative affinities of competing pyrrolopyrimidine inhibitors for FAK kinase. *J Am Chem Soc* 2010;132:3312–3320.
58. Hardré R, Salmon L. Competitive inhibitors of yeast phosphoglucose isomerase: synthesis and evaluation of new types of phosphorylated sugars from the synthon D-arabinolactone-5-phosphate. *Carbohydr Res* 1999;318:110–115.
59. Chirgwin JM, Noltmann EA. The enediolate analogue 5-phosphoarabinonate as a mechanistic probe for phosphoglucose isomerase. *J Biol Chem* 1975;250:7272–7276.
60. Hardré R, Bonnette C, Salmon L, Gaudemer A. Synthesis and evaluation of a new inhibitor of phosphoglucose isomerase: the enediolate analogue 5-phospho-D-arabinohydroxamate. *Bioorg Med Chem Lett* 1998;8:3435–3438.
61. Salmon L, Prost E, Merienne C, Hardré R, Morgant G. A convenient synthesis of aldonohydroxamic acids in water and crystal structure of L-erythronohydroxamic acid. *Carbohydr Res* 2001;335:195–204.

62. Van Schaftingen E, Jaeken J. Phosphomannomutase deficiency is a cause of carbohydrate-deficient glycoprotein syndrome type I. *FEBS Lett* 1995;377:318–320.
63. Noltmann EA. Phosphoglucose isomerase: rabbit muscle (crystalline). *Methods Enzymol* 1966;9:557–565.
64. Piquemal J, Gresh N, Giessner-Prettre C. Improved formulas for the calculation of the electrostatic contribution to the intermolecular interaction energy from multipolar expansion of the electronic distribution. *J Phys Chem A* 2003;107:10353–10359.
65. Piquemal J, Chelli R, Procacci P, Gresh N. Key role of the polarization anisotropy of water in modeling classical polarizable force fields. *J Phys Chem A* 2007;111:8170–8176.
66. Piquemal J, Chevreaux H, Gresh N. Toward a separate reproduction of the contributions to the Hartree–Fock and DFT intermolecular interaction energies by polarizable molecular mechanics with the SIBFA potential. *J Chem Theory Comput* 2007;3:824–837.
67. Claverie P, Daudey JP, Langlet J, Pullman B, Piazzola D, Huron MJ. Studies of solvent effects. I. Discrete, continuum, and discrete-continuum models and their comparison for some simple cases: ammonium(1+) ion, methanol, and substituted ammonium(1+) ion. *J Phys Chem* 1978;82:405–418.
68. Thompson JD, Higgins DG, Gibson TJ. CLUSTAL W: improving the sensitivity of progressive multiple sequence alignment through sequence weighting, position-specific gap penalties and weight matrix choice. *Nucleic Acids Res* 1994;22:4673–4680.
69. Combet C, Blanchet C, Geourjon C, Deléage G. NPS@: network protein sequence analysis. *Trends Biochem Sci* 2000;25:147–150.
70. Gouet P, Robert X, Courcelle E. ESPript/ENDscript: extracting and rendering sequence and 3D information from atomic structures of proteins. *Nucleic Acids Res* 2003;31:3320–3323.
71. Accelrys. DS visualizer. San Diego, USA: Accelrys Software Inc.; 2005.
72. Persistence of Vision Raytracer. Persistence of Vision Raytracer, Version 3.62. Williamstown, Victoria, Australia: Persistence of Vision Pty Ltd.; 2004.
73. GIMP. GNU image manipulation program, Version 2.6. The GIMP Team; Boston, MA, 2001.
74. Jenkins LMM, Hara T, Durell SR, Hayashi R, Inman JK, Piquemal J, Gresh N, Appella E. Specificity of acyl transfer from 2-mercapto-benzamide thioesters to the HIV-1 nucleocapsid protein. *J Am Chem Soc* 2007;129:11067–11078.
75. Cantor SM, Peniston QP. The reduction of aldoses at the dropping mercury cathode: estimation of the aldehyde structure in aqueous solutions. *J Am Chem Soc* 1940;62:2113–2121.
76. Lee JH, Chang KZ, Patel V, Jeffery CJ. Crystal structure of rabbit phosphoglucose isomerase complexed with its substrate D-fructose 6-phosphate. *Biochemistry* 2001;40:7799–7805.
77. Solomons JTG, Zimmerly EM, Burns S, Krishnamurthy N, Swan MK, Krings S, Muirhead H, Chirgwin J, Davies C. The crystal structure of mouse phosphoglucose isomerase at 1.6 Å resolution and its complex with glucose 6-phosphate reveals the catalytic mechanism of sugar ring opening. *J Mol Biol* 2004;342:847–860.
78. Lee JH, Jeffery CJ. The crystal structure of rabbit phosphoglucose isomerase complexed with D-sorbitol-6-phosphate, an analog of the open chain form of D-glucose-6-phosphate. *Protein Sci* 2005;14:727–734.
79. Roos AK, Burgos E, Ericsson DJ, Salmon L, Mowbray SL. Competitive inhibitors of *Mycobacterium tuberculosis* ribose-5-phosphate isomerase B reveal new information about the reaction mechanism. *J Biol Chem* 2005;280:6416–6422.
80. Maple J, Dinur U, Hagler AT. Derivation of force field for molecular mechanics and dynamics from *ab initio* energy surfaces. *Proc Natl Acad Sci USA* 1988;85:5350–5354.
81. Li H, Robertson AD, Jensen JH. Very fast empirical prediction and rationalization of protein pK_a values. *Proteins* 2005;61:704–721.
82. Bas DC, Rogers DM, Jensen JH. Very fast prediction and rationalization of pK_a values for protein-ligand complexes. *Proteins* 2008;73:765–783.
83. Advanced Chemistry Development Labs. ACD/Chemsketch, Version 12.01. Toronto, Canada: Advanced Chemistry Development Labs, Inc.; 2009.